Title

INFLUENCE OF CHAMBER LENGTH AND EQUIVALENCE RATIO ON FLAME PROPAGATION IN A CONSTANT VOLUME DUCT

Authors

Steinert, W.
Dunn-Rankin, D.
Sawyer, R.F.

Publication Date

1982-09-01

Lawrence Berkeley Laboratory
UNIVERSITY OF CALIFORNIA

ENERGY & ENVIRONMENT DIVISION

To be presented at the Western States Section/
Combustion Institute, Sandia Laboratory, Livermore,
CA, October 11-12, 1982

INFLUENCE OF CHAMBER LENGTH AND EQUIVALENCE RATIO ON FLAME PROPAGATION IN A CONSTANT VOLUME DUCT

W. Steinert, D. Dunn-Rankin, and R.F. Sawyer

September 1982

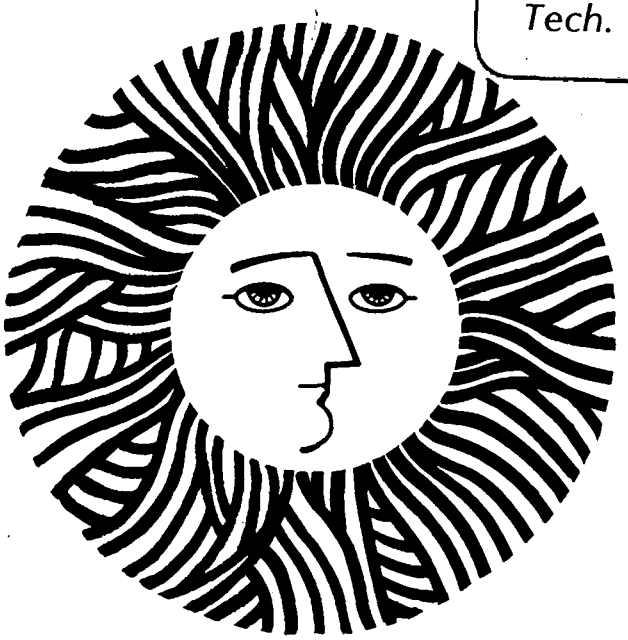

Prepared for the U.S. Department of Energy under Contract DE-AC03-76SF00098

DISCLAIMER

WSS/CI Paper No. 82-72

INFLUENCE OF CHAMBER LENGTH AND EQUIVALENCE RATIO ON FLAME PROPAGATION IN A CONSTANT VOLUME DUCT

W. Steinert*, D. Dunn-Rankin, and R.F. Sawyer

Mechanical Engineering Department and
Energy and Environment Division, Lawrence Berkeley Laboratory
University of California
Berkeley CA 94720

*Institut fuer Physikalische Chemie der Universitaet Goettingen, Visiting Research Scholar

This work was supported by the Lawrence Berkeley Laboratory under U.S. Department of Energy Contract DE-AC03-76SF00098. Support for W. Steinert was provided by the Deutsche Forschungsgemeinschaft.

ABSTRACT

An investigation of flames propagating in a constant volume duct of square cross-section (38 mm by 38 mm) is reported. Two borosilicate glass windows provide full optical access to the combustion process. A line ignition source creates an approximately two-dimensional flame front. The relations among pressure, flame shape, flame speed, and mass consumption rate are examined.

The investigation of flame characteristics is made for 1) stoichiometric methane-air flame propagation in ducts of lengths from 30 mm to 150 mm and 2) ethylene-air flames with equivalence ratios from 0.6 to 1.1 propagating in a 150 mm duct.

Uncertainties in the experimental approach are investigated and traced to deviations in the flame from its assumed two-dimensional shape and to the sensitivity of the flame speed calculation during the flame initiation period to noise in the pressure data.

Results point to distinct regions of flame development, labeled cylindrical, planar, and folded. A correlation between flame shape development and flame speed is noted. The time to peak pressure for the methane experiments is a linear function of duct length. This indicates that despite the distinct flame development regions, the mean mass consumption rate is not sensitive to flame shape variations.

Ethylene flames are found to demonstrate the same general characteristics as the methane flames. The ethylene flame propagation rates are found to be about twice as fast as methane flame propagation rates. The folded ethylene flames exhibit a greater amount of turbulence than comparable methane flames. At low equivalence ratios buoyancy alters the ethylene flame shape.

INTRODUCTION

This investigation is part of a study of the fundamental processes important to the combustion of lean homogeneous mixtures in reciprocating internal combustion engines. Flame propagation in an enclosure is strongly influenced by wall interactions, the size of the combustion chamber, fuel, and equivalence ratio. The main interest focuses on lean mixtures because lean combustion is a promising approach for the improvement of fuel economy and reduction of emissions (Dale and Oppenheim, 1982). However, the application of lean combustion to engines still encounters difficulties related to ignition reliability,

flame speed reduction, increased cyclic variations, and increased hydrocarbon emissions as the lean limit is approached (Shiomoto, et al. 1978; Naguchi, et al. 1976). Recent work on lean engines may be found in IME, 1979.

Experiments conducted in a square cross section constant volume duct are reported. The square cross section was chosen to allow the use of flat windows as side walls and a constant volume was employed because an understanding of combustion under these idealized conditions was sought before progressing to the more complex case of a moving piston. In previous studies the influence of equivalence ratio on methane flame propagation at a fixed duct length was studied (Woodard, et al. 1981) and flame propagation near the lean limit in an expanding chamber was investigated (Smith, et al. 1979). The present study is concerned with the influence of chamber length on flame propagation in a stoichiometric methane/air mixture. Additionally, the earlier methane/air flame propagation studies at a fixed duct length and varying equivalence ratio are repeated with ethylene as the fuel. Ethylene/air has a laminar flame speed approximately twice that of methane/air and therefore allows comparison of two fuels with significantly different combustion properties.

EXPERIMENTAL APPROACH

Measurements are conducted in the constant volume mode of a compression-expansion apparatus (CE-I) which is designed to provide full optical access to combustion events simulating those occurring in reciprocating internal combustion engines. The main features of this apparatus are described here; a more detailed description may be found in Oppenheim, et al. (1976) and Smith (1977).

The experimental apparatus and instrumentation are described in Figure 1. The test section consists of a horizontal duct with a square cross section 38.1 mm by 38.1 mm. It is enclosed on both vertical sides by optical quality borosilicate glass windows and on the top and bottom by steel walls each of which includes two access ports for instrumentation and gas transfer. One endwall is a movable aluminum piston sealed with two teflon rings. The endwall opposite the piston contains a line ignition system.

The fuel/air mixture is delivered by a gas mixing device which controls the equivalence ratio by flow rotameters. The rotameters are calibrated with soap bubble meters and the uncertainty in the equivalence ratio is estimated to be about 5%. For better purging the inlet gas valve is placed close to the igniter on the top, while the exhaust gas valve is placed close to the piston and on the

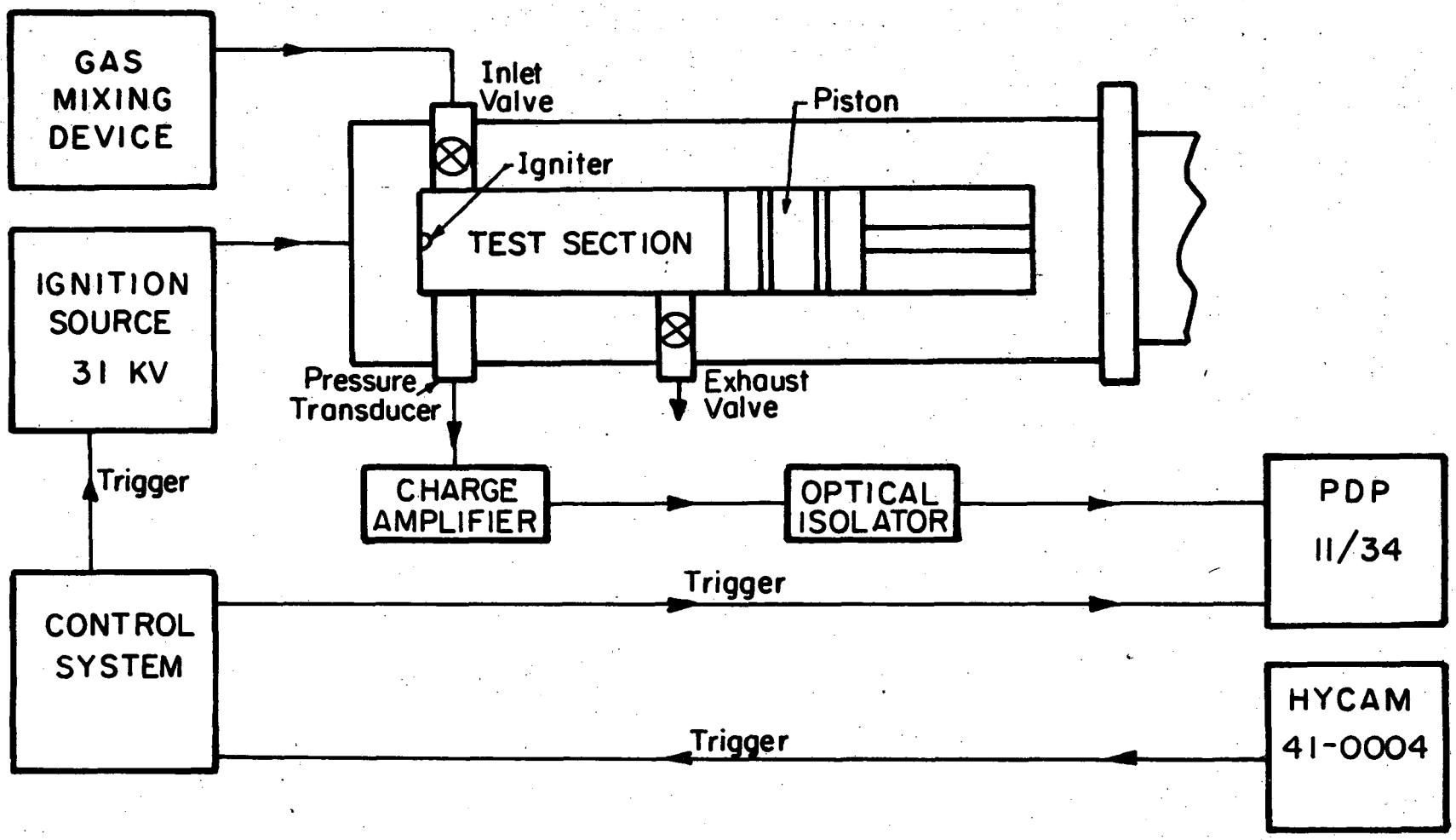

Figure 1. Schematic of experimental apparatus.

bottom. For short chamber lengths the reduced number of access ports available requires that a small exhaust port in the inlet valve be used. To insure a uniform mixture, the chamber is flushed for at least two minutes at a flow of 50 to 80 cm^3/s before each experiment.

The line igniter system consists of a row of fifteen 0.51 mm spark gaps formed by brass electrodes filed to a knife edge. The row of electrodes is mounted in the test section running horizontally from window to window to obtain flame uniformity in the direction perpendicular to the windows. The ignition energy source is a 130 picoFarad capacitor initially charged to 31 kV. The stored energy is dissipated in a trigger air gap (20 mm) and across the line igniter. Assuming that energy dissipation is proportional to gap length, the ignition energy is approximately 20 mJ.

The propagation of the two dimensional flame into the unburned fuel/air mixture is observed with a high speed schlieren system in a Z-configuration, Figure 2, using two concave mirrors of 3.94 m focal length. The combination of a point light source (Oriel xenon lamp, model 6140, at 25 amps with a 2.0 mm hole) and the first mirror provide parallel light through the test section. This light is gathered by the second mirror, passed through a vertical schlieren knife edge stop, and is recorded with a high speed camera (Hycam Model 41-0004, about 5400 frames/s, Kodak Tri-X-Reversal film).

During and shortly after the combustion event, the chamber pressure is measured using a piezoelectric transducer (AVL 12QP300 cvk#1402, sensitivity 42.04 pc/bar, linearity to within one percent, natural frequency 60 kHz, damping 0.25) located in the front access port just below the line ignition source. The signals are amplified by a charge amplifier (Kistler 504E 513 154, medium time constant). The calibration of the tranducer/amplifier combination was dynamically verified in a shock tube. The pressure data are sampled every 0.2 ms by a PDP 11/34 computer using an AR-11 analog to digital converter. The computer and the charge amplifier are connected by an optical isolator to protect the computer from harmful ground loops and peak currents caused by the igniter.

The ignition source and computer are triggered and synchronized by the high-speed camera through the control panel. The event is triggered when the high speed camera reaches operating speed.

With the above described apparatus, constant volume combustion experiments are conducted which involve simultaneously measuring the pressure and photographing the flame. In all measurement the initial conditions are atmospheric pressure and ambient temperature. Methane (99.99%) and ethylene (98.5% ethylene, 0.4% methane, 1.0%

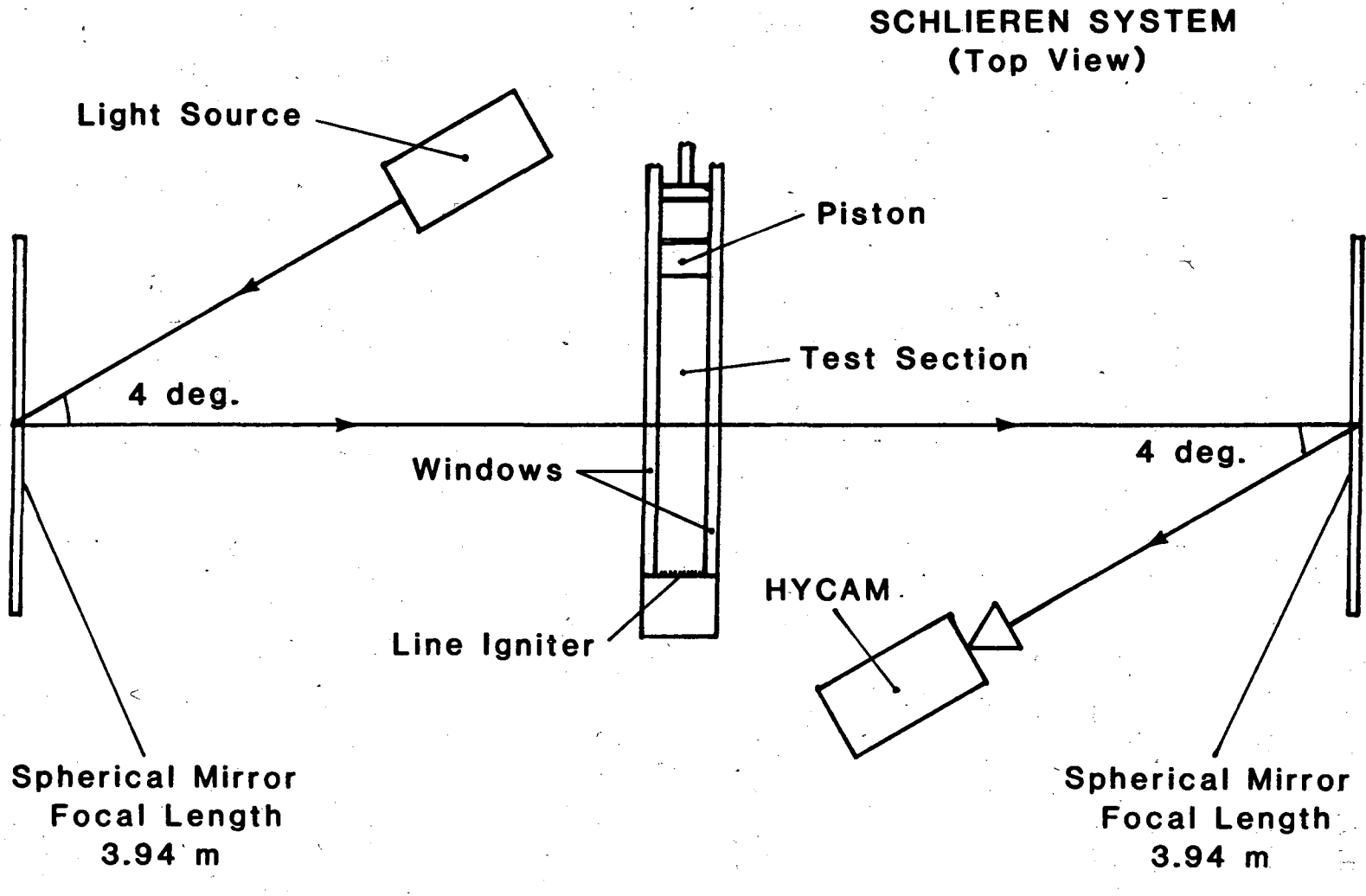

Figure 2. Schematic of schlieren system.

ethane, 0.1% propane) are used as fuels with air as oxidizer. For methane experiments the equivalence ratio is kept constant at 1.0 and the chamber length varied (30, 60, 90, 120, 150 mm). With ethylene the chamber length is kept constant at 150 mm and the equivalence ratio varied (0.6, 0.7, 0.8, 0.9, 1.0, 1.1).

DATA ANALYSIS FOR FLAME SPEED AND MASS BURNING RATE

Pressure and digitized flame front locations are used to calculate an effective flame velocity and mass consumption rate as a function of time. These calculations are based on the following assumptions:

1) No net heat flux occurs across the boundaries of the unburned gases.
2) The flame front is negligibly thin.
3) The unburned gas behaves as an inviscid ideal gas of constant specific heat ratio and composition corresponding to that of the initial mixture.
4) The pressure is spatially uniform inside the combustion chamber.

The acceptability of these assumptions has been demonstrated by Smith (1977). He also showed that the flame speed may be expressed as:

$$S_u = \frac{-V_u}{A_f} \left(\frac{1}{\gamma P} \frac{\partial P}{\partial t} + \frac{1}{V_u} \frac{\partial V_u}{\partial t} \right) \qquad (1)$$

where, A_f = flame area, V_u = volume unburned, γ = ratio of specific heats of unburned mixture, P = chamber pressure, and t = time. The mass burning rate is then:

$$\dot{m} = \frac{P_o^{\left(\frac{\gamma-1}{\gamma}\right)}}{RT_o} P^{\left(\frac{1}{\gamma}\right)} V_u \left(\frac{1}{\gamma P} \frac{\partial P}{\partial t} + \frac{1}{V_u} \frac{\partial V_u}{\partial t} \right) \qquad (2)$$

where P_o = initial pressure and T_o =initial temperature.

The unburned volume, its derivative, and the flame area are all determined from digitized high speed schlieren movies. This determination is non-trivial due to the schlieren images being excessively broad and improperly representative of a two-dimensional flame sheet. The front of the broad schlieren image extinguishes at the endwall before the pressure reaches its peak. This indicates that the front of the schlieren image is not an accurate representation of the true flame front. The rear of the schlieren image disappears at the endwall after the pressure peaks. Heat and leak losses may account for the delay between pressure peak and rear flame arrival, but negative flame speeds and back-tracking of the schlieren image, Figures 3 and 4, preclude use of the rear schlieren alone as the true flame front. Color schlieren, using a bulls-eye stop for deflection marking, indicate a

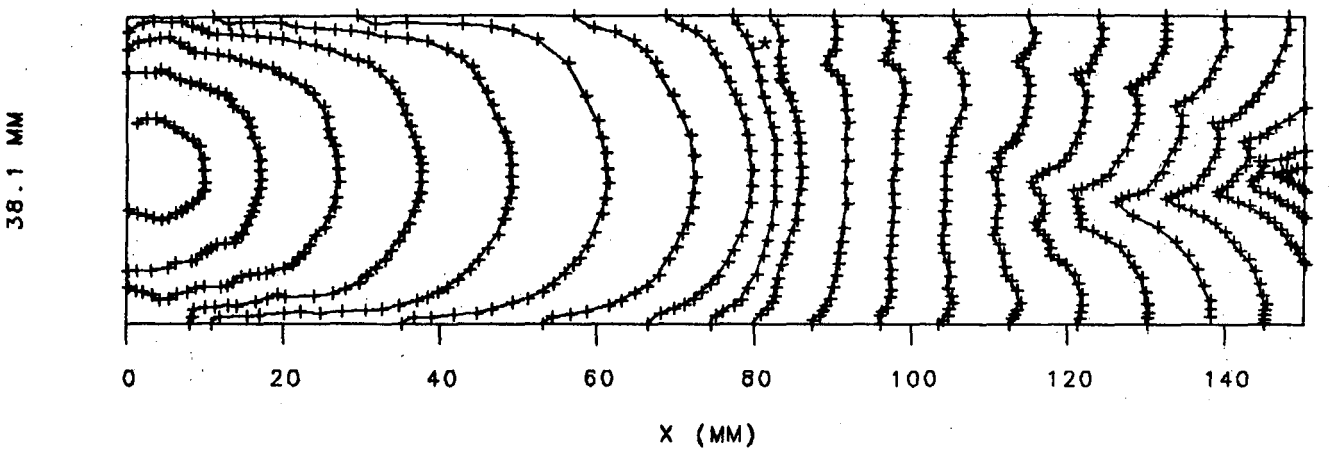

a) Front of schlieren image.

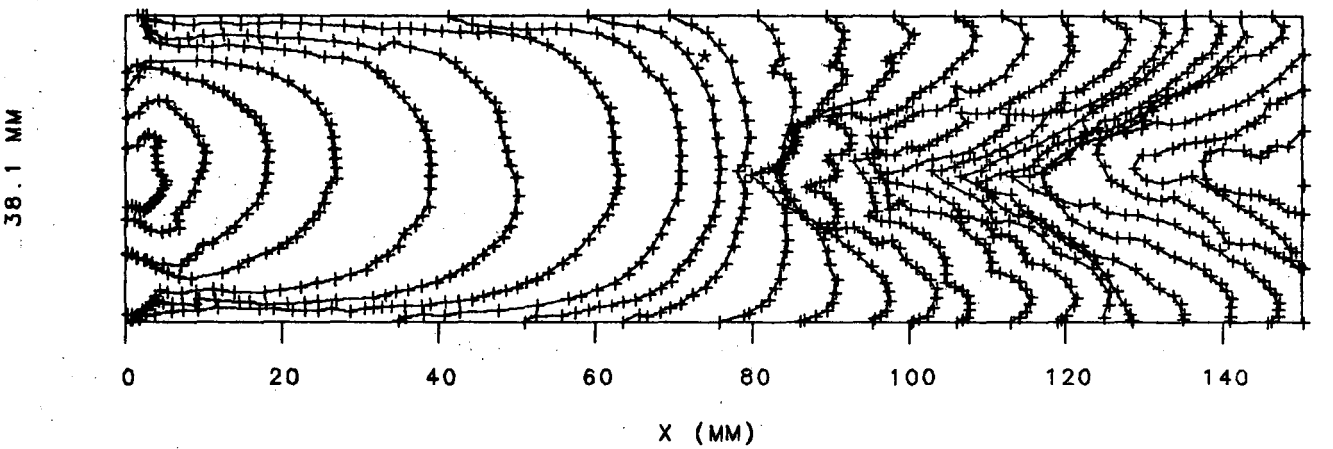

b) Rear of schlieren image.

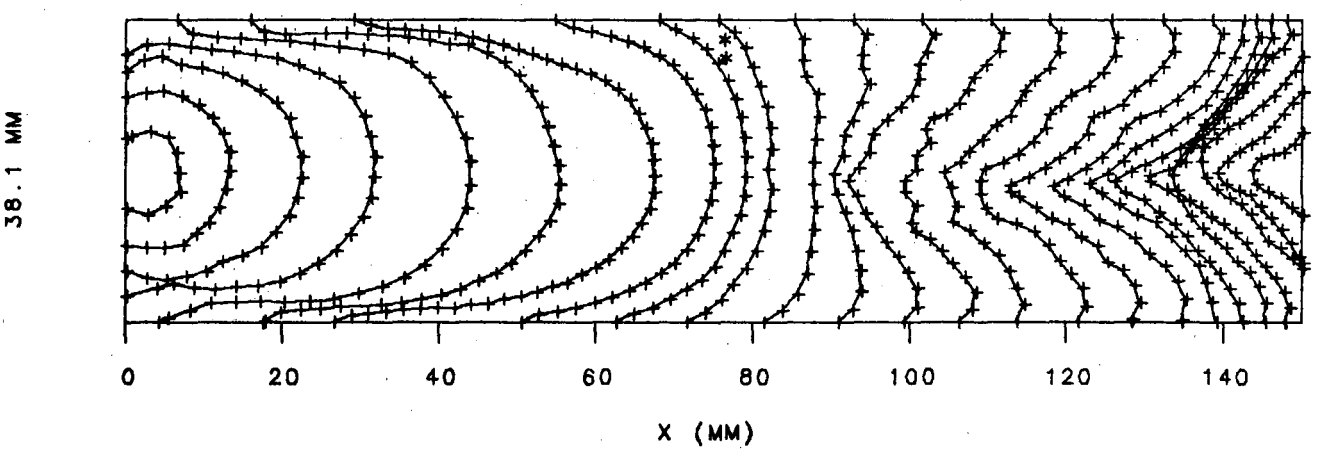

c) Average flame shape.

Figure 3. Comparison of a) front, b) rear and c) average digitized flame shapes. Methane/air flame equivalence ratio 1.0; duct length 150 mm; time step between flame shape contours 1.85 ms to * then 3.70 ms.

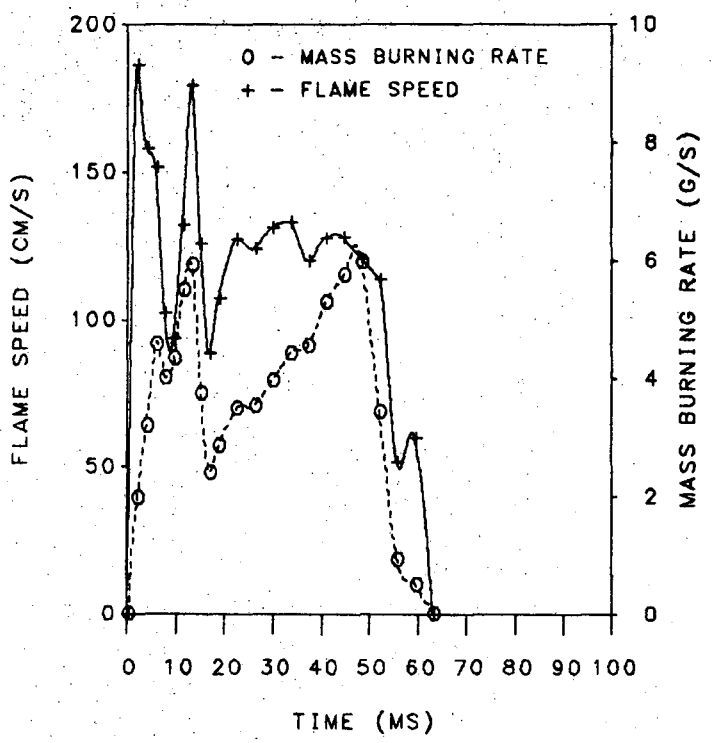

a) Front of schlieren image.

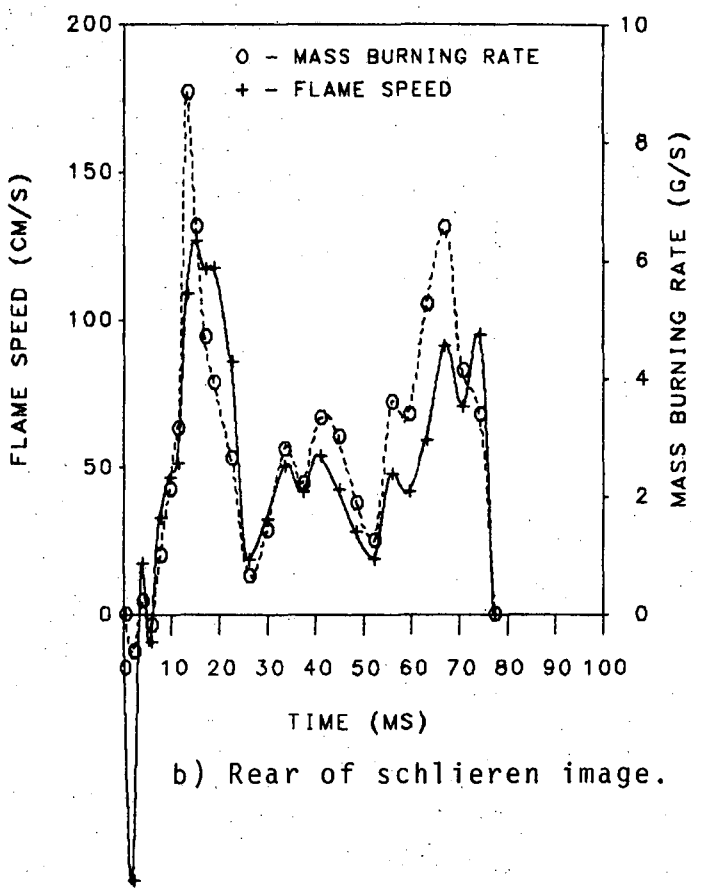

b) Rear of schlieren image.

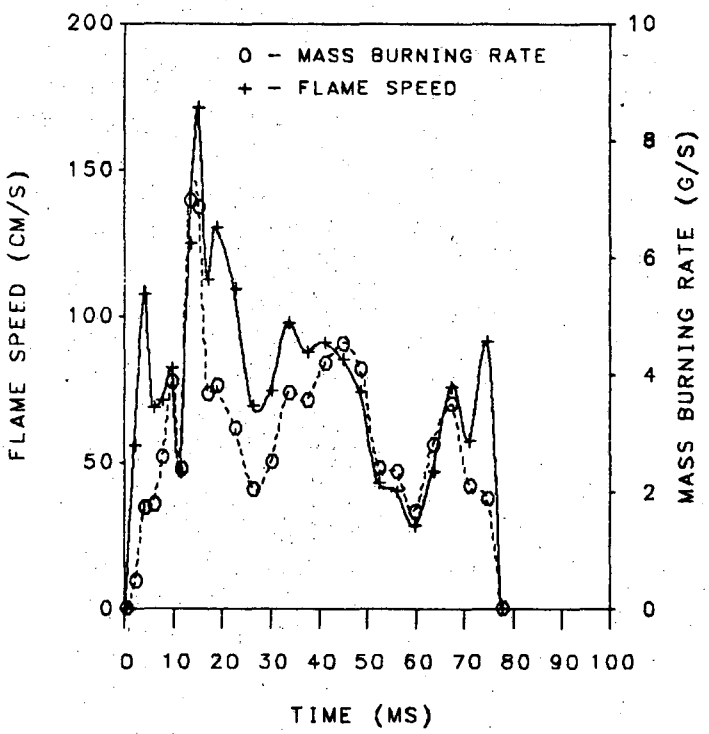

c) Average schlieren image.

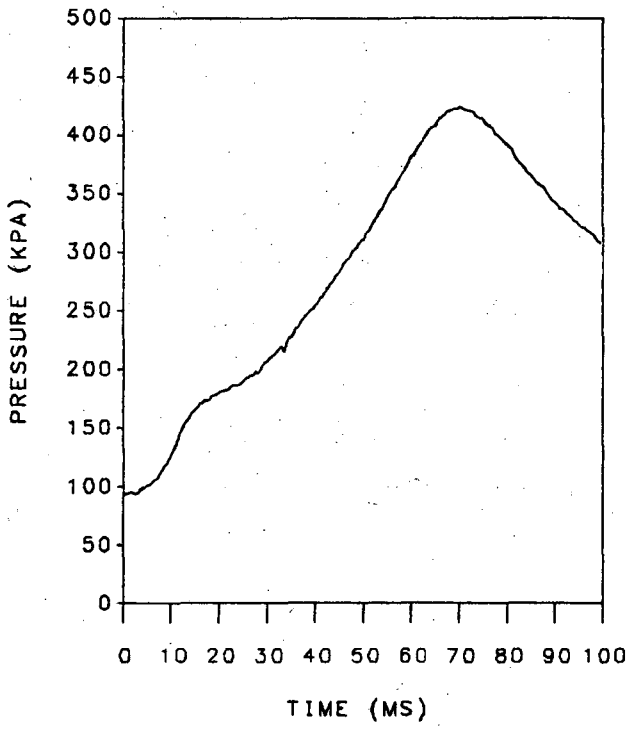

d) Pressure.

Figure 4. Comparison of flame speed and mass burning rates obtained using the a) front, b) rear and c) average schlieren image. Methane/air flame: equivalence ratio 1.0; duct length 150 mm.

three-dimensional flame structure. Because of the inherent line of sight integration in the schlieren technique precise three-dimensional flame shape can not be determined. To approximate the three-dimensional flame shape, an average flame front is defined to give a more accurate description of the unburned volume in the duct, Figure 3. As can be seen from Equation (1), for even qualitatively correct flame speed results, proper representation of unburned volume is essential.

The flame average is found by first digitizing both the leading and trailing edges of the schlieren image. The points on these tentative flame fronts are then replaced by new points equidistantly spaced along the fronts such that there are the same number of points on both the leading and trailing images. A point by point average is then taken. Once the front schlieren image disappears at the end of the duct, the rear flame is averaged with the endwall. The set of average points defines the expected mean flame, Figure 3. The flame area is computed by summing the distance between successive co-ordinate pairs representing the flame. The volume is determined by a trapezoidal integration behind the connected points. Points are spaced at equal intervals, 2 mm, along the flame. The spacing is small enough so that the error due to the use of straight line segments is negligible. It should be noted that the average flame is designed to give a more accurate description of the unburned volume and does not necessarily accurately describe the true flame area. Possible error in flame area using digitized schlieren movies has been found to be as much as 100% (Smith, 1977). The volumes obtained from the average digitized flame front are fitted with a cubic spline using an IMSL (International Mathematics and Statistics Library) routine (ICSSCU). The derivative of the spline gives the instantaneous dV_u/dt value required for flame speed calculations.

Using the flame speed assumptions given at the beginning of this section, the accuracy of the volume burned defined by the flame position average was checked for the early post-ignition flame. Beginning with the ideal gas law, in both the burned and unburned medium,

$$P_u V_u = n_u R T_u \; ; \; P_b V_b = n_b R T_b \; ; \; P_o V_o = n_o R T_o \qquad (3)$$

where u = unburned gas, b = burned gas, o = initial, n = mole number, R = universal gas constant. Assuming constant pressure, $P_u = P_b = P$, and $\sum n_i = n_o$,

$$\frac{T_u}{T_b}\left(\frac{V_o - V_u}{V_u}\right) = \left(\frac{P_o}{P}\right)\left(\frac{V_o}{V_u}\right)\left(\frac{T_u}{T_o}\right) - 1 \qquad (4)$$

Letting the unburned gas undergo adiabatic compression,

$$T_u = T_o \left(\frac{P}{P_o}\right)^{\left(\frac{\gamma-1}{\gamma}\right)} \qquad (5)$$

Substituting and rearranging

$$\left(\frac{P}{P_o}\right)^{\left(\frac{1}{\gamma}\right)} \left(\frac{V_u}{V_o}\right) + \left(\frac{T_o}{T_b}\right) \frac{P}{P_o} \left(1 - \frac{V_u}{V_o}\right) = 1 \qquad (6)$$

Initially, $T_o << T_b$, $V_u \approx V_o$, and $P \approx P_o$ and with these approximations,

$$\left(\frac{V_u}{V_o}\right) \approx \left(\frac{P}{P_o}\right)^{-\left(\frac{1}{\gamma}\right)} \qquad (7)$$

The recorded pressure data are in good agreement with the pressures computed using the average flame volume in (7). The agreement is assumed good throughout the combustion but can not be checked due to uncertainties in (7) arising from the neglected and increasingly important burned gas temperature information.

Inconsistencies in the flame speeds computed for the early post-ignition period result primarily from inaccuracies in dP/dt generated by ignition noise. The noise has little effect on the pressure data itself, less than 3%, but is sufficient to create extremely large errors in dP/dt. Often dP/dt in the noisy region is found to be negative. To reduce the effect of the noise, Figure 5a, the pressure data are smoothed with an IMSL smoothing spline routine (ICSSCU) allowing a user-specified smoothing parameter to control the extent of smoothing. dP/dt is then found using the IMSL spline derivative evaluator (DCSEVU). With a smoothing parameter sufficient to insure non-negative pressure slope, the maximum deviation of the smoothed pressure from the original data does not exceed two percent. This value corresponds to a smoothing parameter of approximately 0.6 per pressure point.

The smoothed pressure data occasionally demonstrate pressure rate increases that are abnormally large in comparison with the rate of volume change. This causes the first bracketed term in Equation (1) to dominate and produces negative flame speeds. In the early post ignition flame, the time rates of change of dP/dt and dV_u/dt (second derivatives of the pressure and volume) are large. Because dP/dt and dV_u/dt come from separate data records their proper syncronization in time is crucial for consistent results. Small changes in the synchronization (0.2 to 1.0 ms) have a very large effect on the initial flame speed, Figure 5b. Later in the combustion, dP/dt and dV_u/dt become roughly constant and the effect of improper synchronization disappears.

To check the early synchronization of dV_u/dt and dP/dt, an initial flame speed expression requiring only volume rate or pressure rate information is derived from Equations (1) and (7). Replacing the variables in (6) with dimensionless variables,

$$\pi = \frac{P}{P_o} \qquad \eta = \frac{V_u}{V_o} \qquad \tau = \frac{T_o}{T_b} \qquad (8)$$

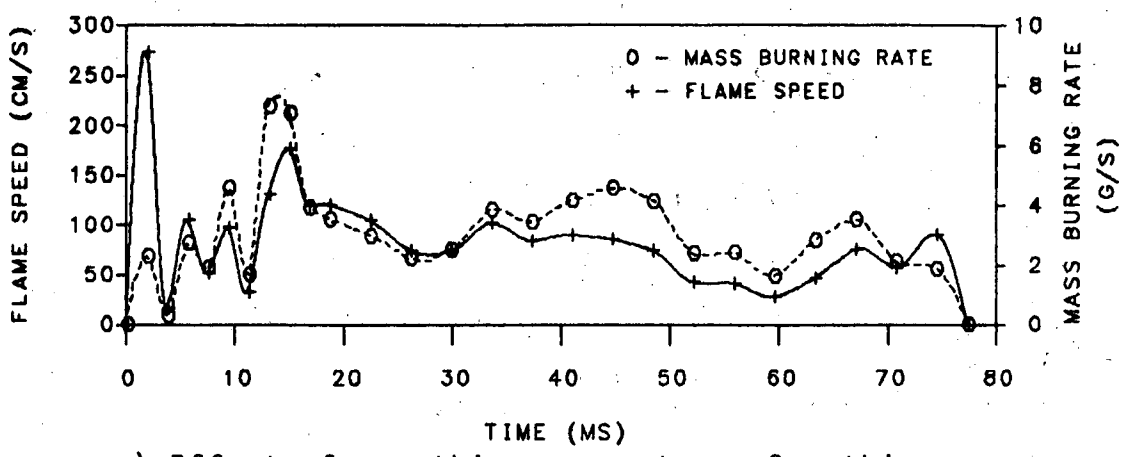

a) Effect of smoothing parameter. Smoothing parameter = 75; delay = 0.

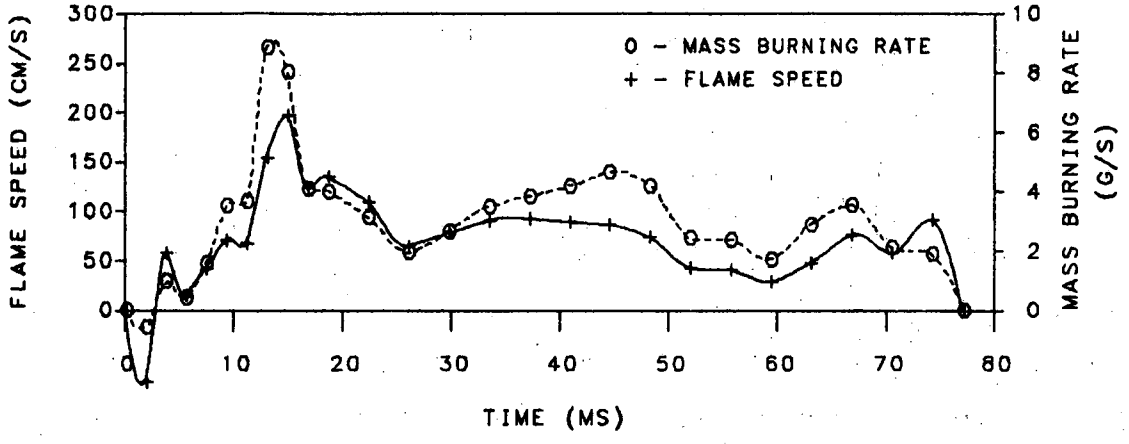

b) Effect of synchronization. Smoothing parameter = 125; delay = 1.0 ms.

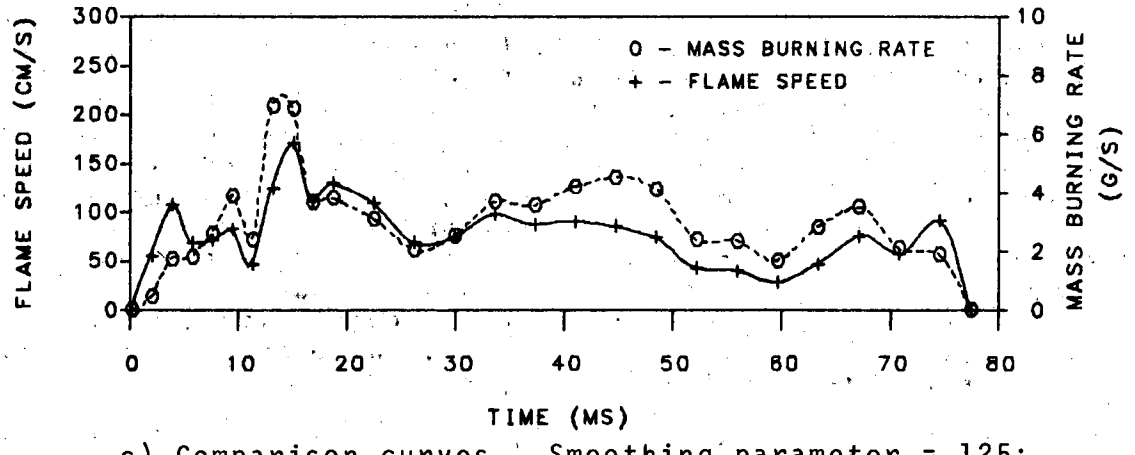

c) Comparison curves. Smoothing parameter = 125; delay = 0.

Figure 5. Effect of a) smoothing pressure data and b) synchronization of pressure and flame shape data on flame speed and mass burning rate. Methane/air flame; equivalence ratio 1.0 duct length 150 mm.

(6) becomes

$$\eta\pi^{(\frac{1}{\gamma})} + \tau\pi\,(1 - \eta) = 1 \qquad (9)$$

Taking the time derivative with τ assumed constant,

$$\frac{\partial\eta}{\partial t}\left(\pi^{(\frac{1}{\gamma})} - \tau\pi\right) + \frac{\partial\pi}{\partial t}\left[(1-\eta)\tau + \frac{\eta}{\gamma}\,\pi^{(\frac{1}{\gamma} - 1)}\right] = 0 \qquad (10)$$

Assuming, $\eta \approx 1$, $\tau << 1$, $\pi \approx 1$, the term $(1 - \eta)\tau$ is neglected. With this assumption and using $\eta \approx \pi^{-(\frac{1}{\gamma})}$ from (7), solving for $\partial\pi/\partial t$ yields

$$\frac{\partial\pi}{\partial t} = -\gamma\pi\left[\pi^{(\frac{1}{\gamma})} - \tau\pi\right]\frac{\partial\eta}{\partial t} \qquad (11)$$

With non-dimensional variables Equation (1) becomes

$$S_u = \frac{-V_o}{A_f}\left[\frac{\pi^{(\frac{1}{\gamma})}}{\gamma\pi}\,\frac{\partial\pi}{\partial t} + \frac{\partial\eta}{\partial t}\right] \qquad (12)$$

Substituting (11) into (12)

$$S_u = \frac{-V_o}{A_f}\left[\tau\pi^{(\frac{\gamma-1}{\gamma})}\right]\frac{\partial\eta}{\partial t} \qquad (13)$$

Initially $\pi \approx 1$ and so

$$S_u \approx \frac{-V_o}{A_f}\,\tau\,\frac{\partial\eta}{\partial t} = \frac{-\tau}{A_f}\,\frac{\partial V_u}{\partial t} \qquad (14)$$

In a similar manner, it can be shown that,

$$S_u \approx \frac{V_o\tau}{A_f\gamma P_o}\,\frac{\partial P}{\partial t} \qquad (15)$$

These expressions have the limitation of validity only in the early flame, but are self-consistent and require no synchronization. Because of the required smoothing there is considerable uncertainty in the dP/dt information in the early post-ignition period and so the expression involving dV_u/dt was used. Results of initial flame speeds for the above expression are in reasonable agreement with previously reported initial ethylene/air flame speeds (de Soete, 1981). These results, however, differ considerably from the results obtained using Equation (1). The uncertainty in the beginning of a combustion event, when the pressure is relatively constant, has been observed by other investigators (Rallis and Garforth, 1980).

To avoid an arbitrary junction between results of Equations (1) and (14) and to allow comparison to previous work on the apparatus, Equation (1) is used exclusively in this work. However, due to 1) lack of self-consistency in the expression, 2) electronic noise in the pressure data, 3) a relatively small flame area contributing a greater precentage error in the flame speed, S_u, 4) rapid changes in dP/dt and dV_u/dt, and 5) sensitivity to slightly

asynchronous data records, large uncertainties exist in the flame speeds during the early post-ignition combustion period. The flame speeds in this period are omitted from the discussion. Near the end of the combustion, problems 3) and 4) reappear, but the other effects seem to have little significance, Figure 5. The results for this region are included in the discussion, but uncertainties are greater than during the bulk of the combustion.

METHANE/AIR FLAME PROPAGATION: EFFECT OF DUCT LENGTH

A study is made of stoichiometric methane/air flames propagating in ducts of lengths ranging from 30 mm to 150 mm. The behavior of flame development is obtained using high speed schlieren movies. Pressure and flame development are correlated. Using schlieren information simultaneously with pressure information, time resolved flame speeds and mass burning rates are computed. Finally, flame speed and flame shape development are compared.

Flame Shape and Development

Flame shape development in closed tube combustion has been discussed by other experimenters, for example, Guenoche (1964). The approximately planar two-dimensional flames in the present study behave very similarly to these closed tube flames. In nearly all cases studied the flame demonstrates three distinct shapes. For ease of reference, they have been labeled, cylindrical, planar, and folded, Figure 6.

1) CYLINDRICAL: In all cases the flame begins as a small semi-cylinder centered on the igniter. Initially the flame expands uniformly, maintaining its semi-cylindrical shape. Then, as the flame nears the side-walls, it takes on an elongated form. The elongation can be described as a semi-cylindrical cap on twin flame legs parallel to the side-walls. The extent of the elongation is a function of duct length, Figure 7. In the 30 mm case there is no noticeable elongation. The elongation first appears in the 60 mm case and grows as the duct length is increased. As the legs burn out the flame resumes an approximately semi-cylindrical shape.

The semi-cylindrical flame form persists for proportionally larger fractions of the duct length as the length is decreased. The semi-cylindrical shape covers just over half of the total duct length for the 150 mm case while remaining in existence for virtually the entire combustion process at 30 mm.

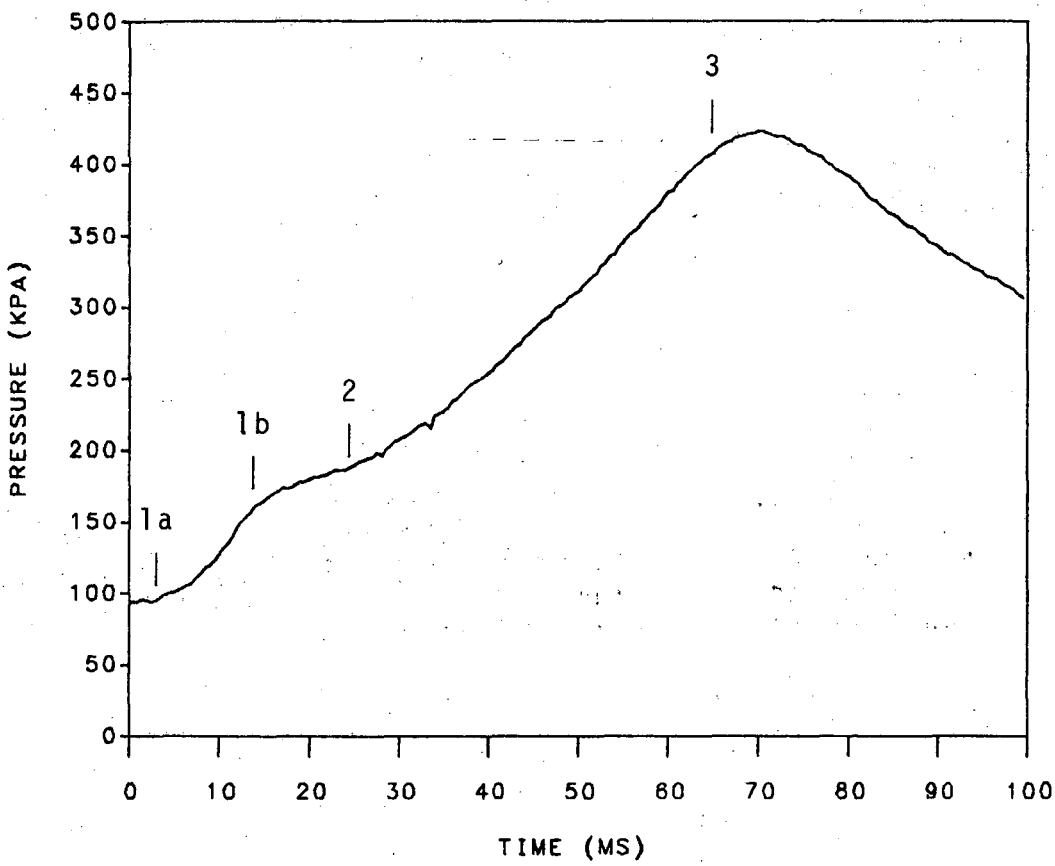

a) Pressure.

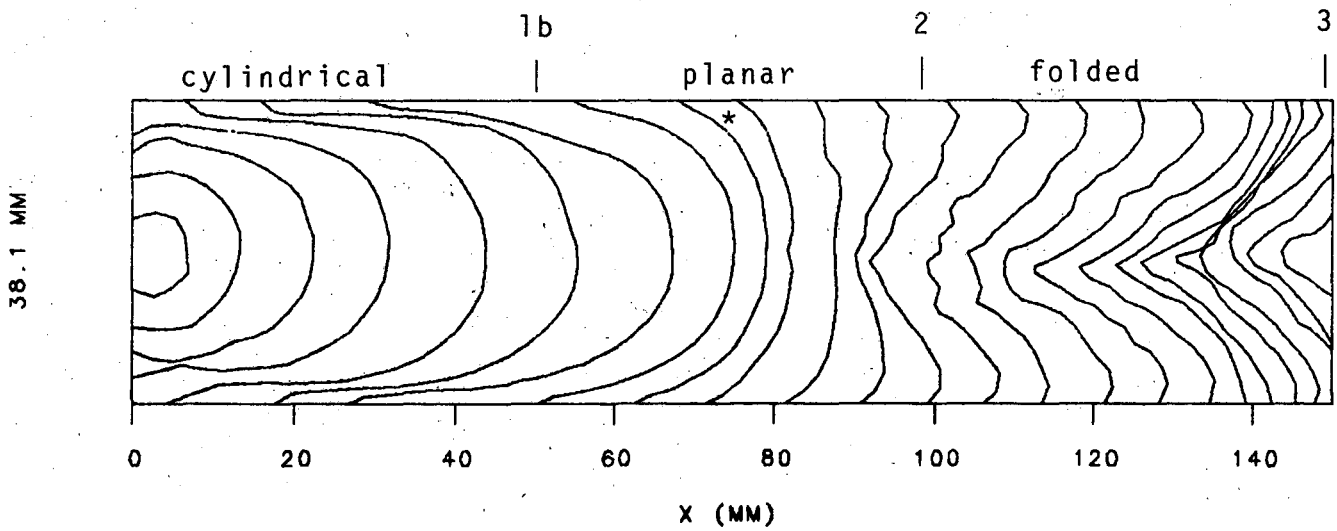

b) Flame shape.

Figure 6. Notable regions of flame shape development and pressure history. Methane/air flame: duct length 150 mm; equivalence ratio 1.0; time step between flame shape contours 1.85 ms to * then 3.70 ms.

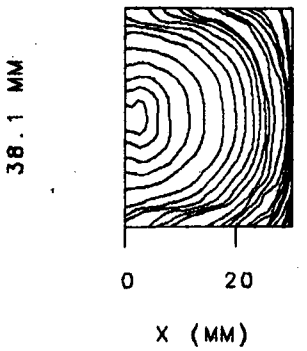

a) Duct length 30 mm; time step between flame shape contours 0.93 ms.

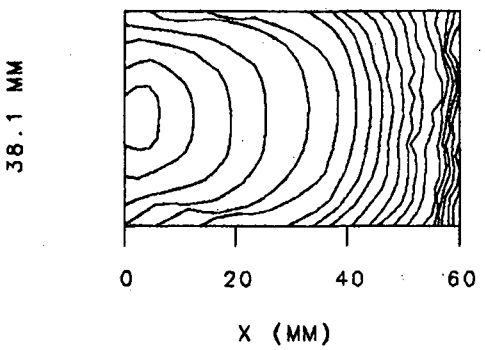

b) Duct length 60 mm; time step between flame shape contours 1.85 ms.

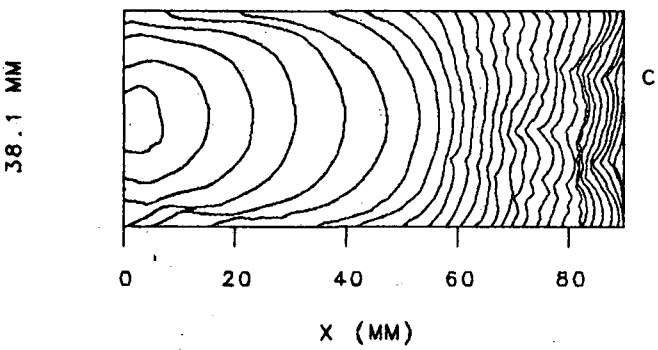

c) Duct length 90 mm; time step between flame shape contours 1.85 ms.

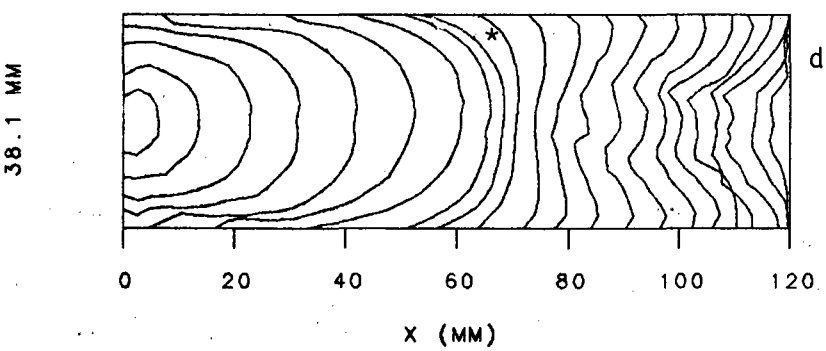

d) Duct length 120 mm; time step between flame shape contour 1.86 ms to * then 3.72 ms.

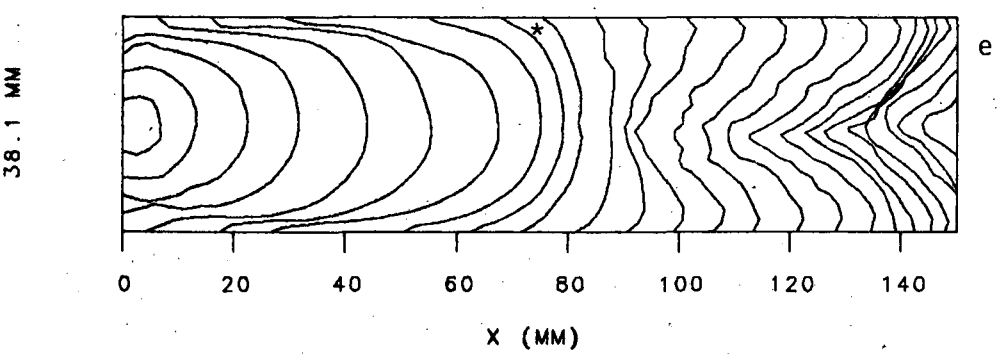

e) Duct length 150 mm; time step between flame shape contours 1.85 ms to * then 3.70 ms.

Figure 7. Flame shape in different length ducts. Methane/air flame; equivalence ratio 1.0.

Judging from the similarity in flame shape obtained from front and rear schlieren images, the flame appears to be nearly two-dimensional during the cylindrical flame period.

2) PLANAR: As the portions of the flame near the side-walls catch up to the centrally burning section, the flame begins to flatten. During this period, the flame has its minimum area (excluding initial and final flame areas). The duration of this planar region varies with duct length. For the 150 mm case the planar region occurs only as a transitional state. The planar flame is increasingly persistent as the duct length diminishes. The 30 mm case is somewhat exceptional, as the planar flame occurs only at the end of combustion.

Schlieren records indicate that the planar flame is nearly two-dimensional.

3) FOLDED: As the flame passes out of the planar stage it progressively folds back in the middle. The folding is most pronounced for larger duct lengths (120 mm and 150 mm). For smaller lengths the folding is more accurately described as undulations in the flame front. There is nearly no undulation in the 30 mm case.

The folding behavior seems to occur coincidentally with a deviation from two-dimensionality. During this period a flame front disturbance increases the flame area. Both the disturbance and deviation from two-dimensional flame character increase as the flame approaches the endwall.

Pressure Change

Pressure information exhibits regions of interest which can be related to the flame shape, Figure 6.

1a) The pressure trace begins with a short flat portion during the flame initiation. The pressure remains approximately constant near the initial pressure. The initial flat corresponds to the time of flame initiation including ignition induction time. Because the induction period does not depend on chamber length, all methane/air pressure data demonstrate the same initial flat period of about 2 ms. The deviation from smooth flatness has been attributed to the previously discussed residual ignition noise.

1b) Following the flat is a steeply increasing region. The steepness of the pressure rise decreases as the chamber length increases. The flame is in the semi-cylindrical stage during this pressure rise and the

flame is not noticeably affected by heat loss to the chamber walls. The flame achieves its maximum area during this period and, because the pressure rise is a strong function of flame area, the pressure increases most dramatically. As chamber volumes decrease, pressure curves steepen due to the more rapid density increase of the unburned gas.

2) Next there occurs a step of high curvature where dP/dt decreases rapidly. The step is increasingly pronounced as the chamber is lengthened. There is no step in the 30 mm case. The step corresponds to the region in which the flame enters the planar form. The drop in dP/dt is due to the vastly reduced flame area as the flame parallel to the walls extinguishes. The lack of step in the 30 mm case is attributable to the flame never becoming planar. The step appears to be strictly a function of flame shape development. This development occurs primarily in the ducts with large length to width ratios.

3) After the step is another steep pressure rise. The pressure rise is not as steep as for 1b) above. dP/dt is nearly constant in this region. Again, the steepness of the pressure curve decreases as the chamber is lengthened. The second rise occurs as the flame area again increases during the folding process. Although the flame area may not be as large as in the semi-cylindrical region, the increase in density of the unburned gas compensates to some extent, giving a higher pressure increase per unit flame area. The decrease in rise steepness with increasing duct length is again due to faster density increases in the shorter ducts. The fact that the pressure rise during this period is not as steep as in the semi-cylindrical flame region is supposed due to reduced flame area along with increased heat loss to the walls and leaks.

4) Finally, the pressure curve flattens, peaks and begins to drop. As the flame burns out, heat losses and leaks cause the pressure to peak and then decay.

In the cases of small duct length (30 mm and 60 mm), the final pressure is found to be lower than atmospheric pressure. The phenomenon is believed due to rapid water condensation and leaks. Condensation is expected to be more rapid at smaller volumes, because of proportionally higher heat losses due to larger surface to volume ratios. Leaks are also proportionally larger for smaller volumes. Because the magnitude of the pressure peaks are nearly equal it is expected that the above described effects, leading to the abnormal final pressure for small volumes, has a negligible effect on the flame propagation of interest.

Flame Speed and Mass Burning Rate

Flame speed is the standard accepted measure of combustion rate in laminar flames. The effects of pressure, temperature, equivalence ratio, and inert gas fraction on the flame speeds of many fuel/oxidizer combinations have been reported. The concept of flame speed also has been applied to turbulent combustion, but the interpretation in this case is not precise. Flame speeds in experiments such as ours are spatially averaged quantities and describe the overall flame propagation. A second combustion rate parameter is the rate at which reactants are consumed, the mass burning rate. The mass burning rate is an integrated quantity and is insensitive in its calculation to the flame geometry. Both parameters are reported and discussed, the flame speed because it is the conventional parameter and the mass consumption rate because it is the more fundamental parameter.

Time resolved flame speed and mass burning rates have been computed, Figures 8-12, for the methane flames previously described. In the present work the mass burning rates are likely to be more accurate than the flame speeds as their computation does not involve the flame area, the least accurate measured quantity. The flame speed generally mimics the mass burning rate, except at the beginning and end of combustion. Therefore, the discussion is mainly in terms of the flame speed to allow comparisons with previous work.

Disregarding the early post ignition period as previously explained, the flame speed results show roughly four or five peaks. The time diffence between the peaks decreases as the duct length decreases. Most results indicate relatively high peaks near the beginning and a single, somewhat smaller peak just before the flame extinguishes.

Distinct correlations between flame speed and flame development are difficult to pinpoint. Some general observations follow:

a) The initial apparent flame speed peak (disregarding the early post ignition period) usually occurs in the transition to planar flame shape. During this period the flame resumes its semi-cylindrical shape after the flame legs have extinguished. The high flame speed results from three mechanisms: 1) reduced flame area during the return to a simple semi-cylindrical shape, 2) smaller dP/dt as the pressure begins its step, and 3) a large dV_u/dt.

b) The drop in flame speed after the first peak coincides with the flame transition to folded shape. This

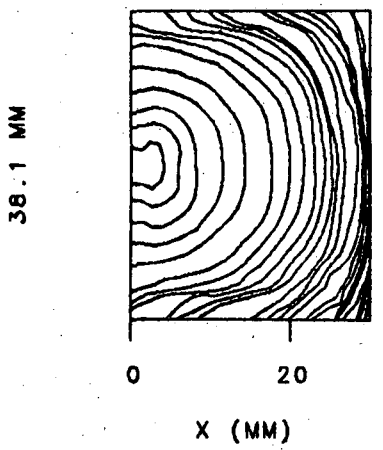

a) Flame shape.

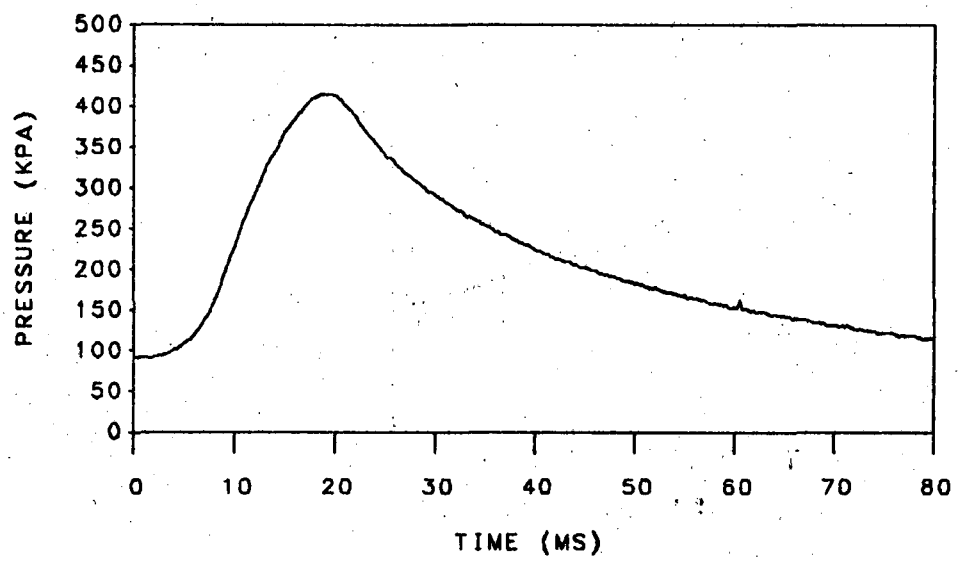

b) Pressure.

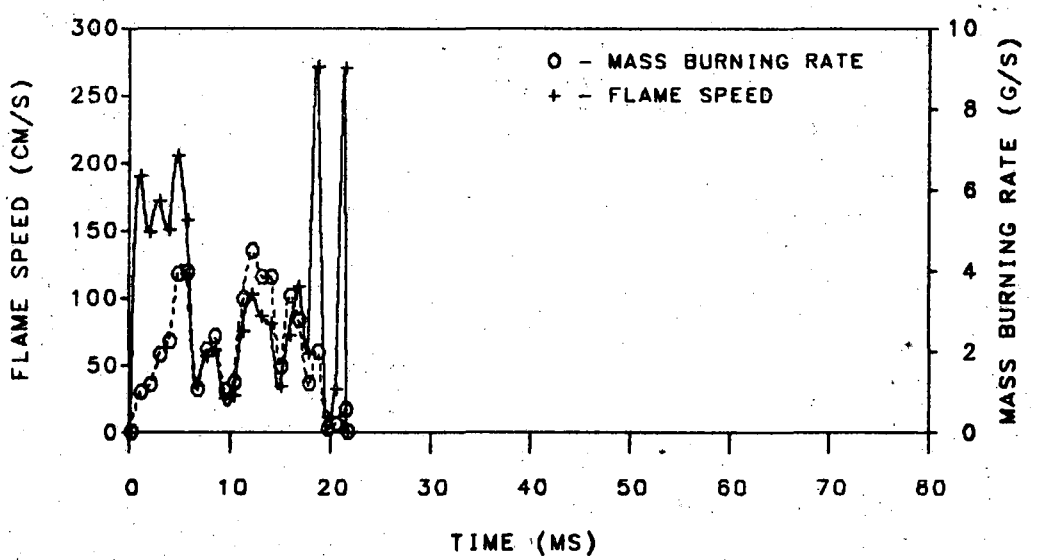

c) Flame speed and mass burning rate.

Figure 8. Methane/air flame results. Duct length = 30 mm, equivalence ratio = 1.0; time step between flame shape contours = 0.93 ms.

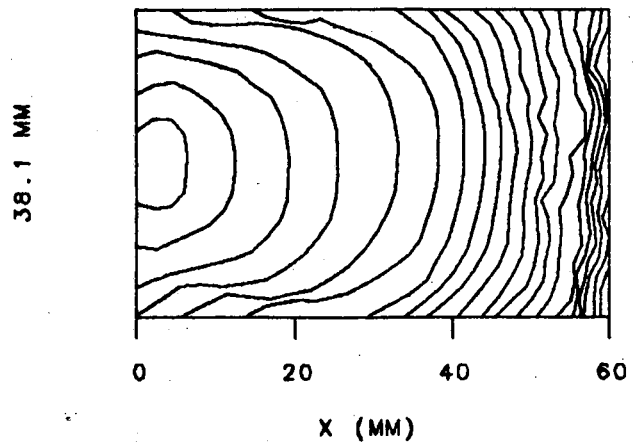

a) Flame shape.

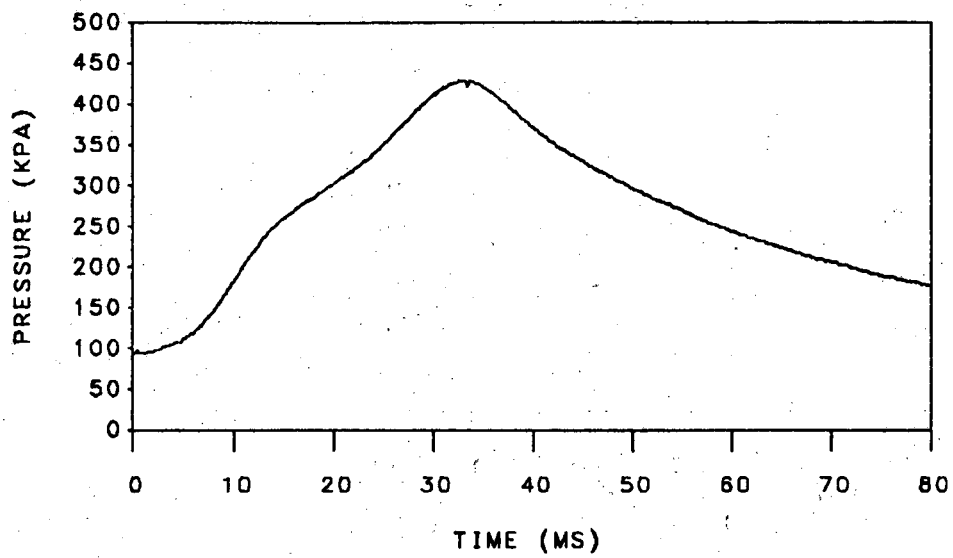

b) Pressure.

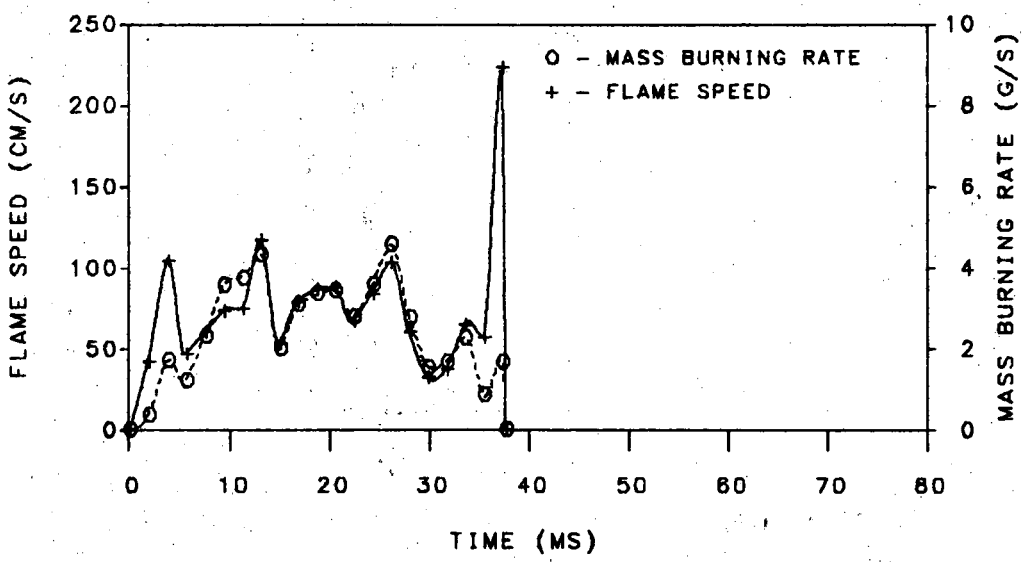

c) Flame speed and mass burning rate.

Figure 9. Methane/air flame results. Duct length = 60 mm; equivalence ratio 1.0; time step between flame shape contours = 1.85 ms.

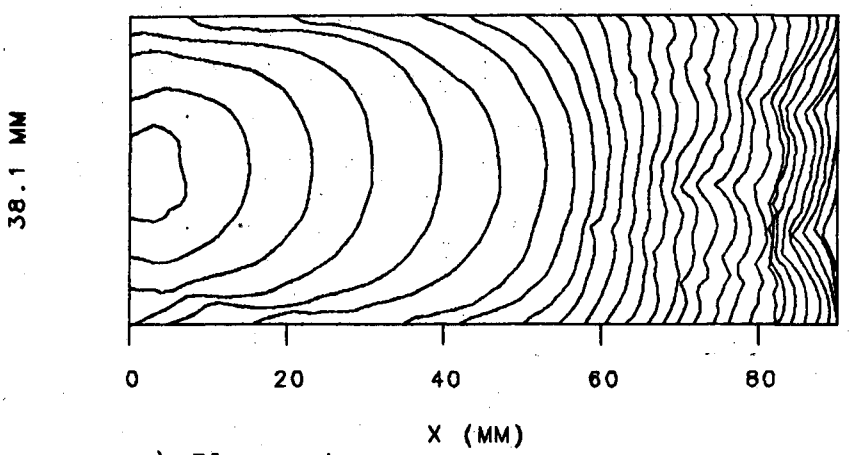

a) Flame shape.

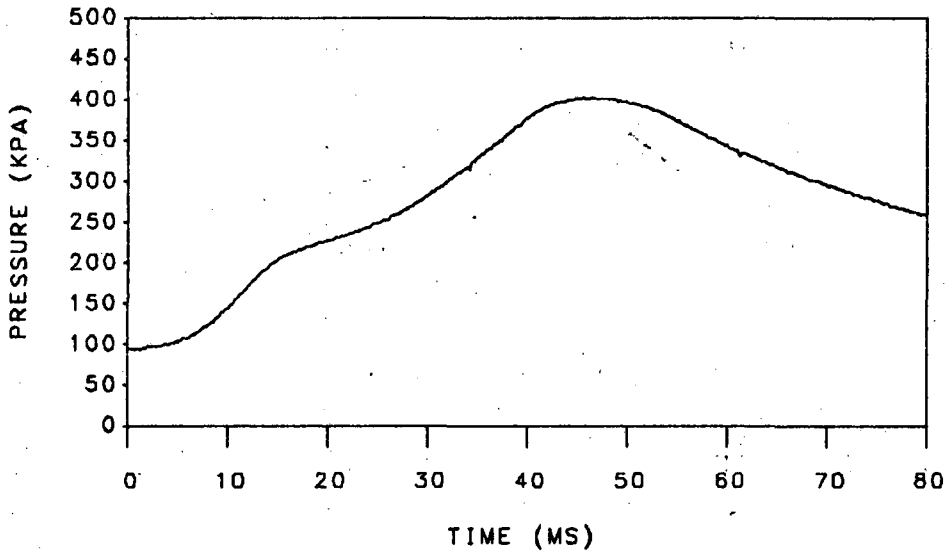

b) Pressure.

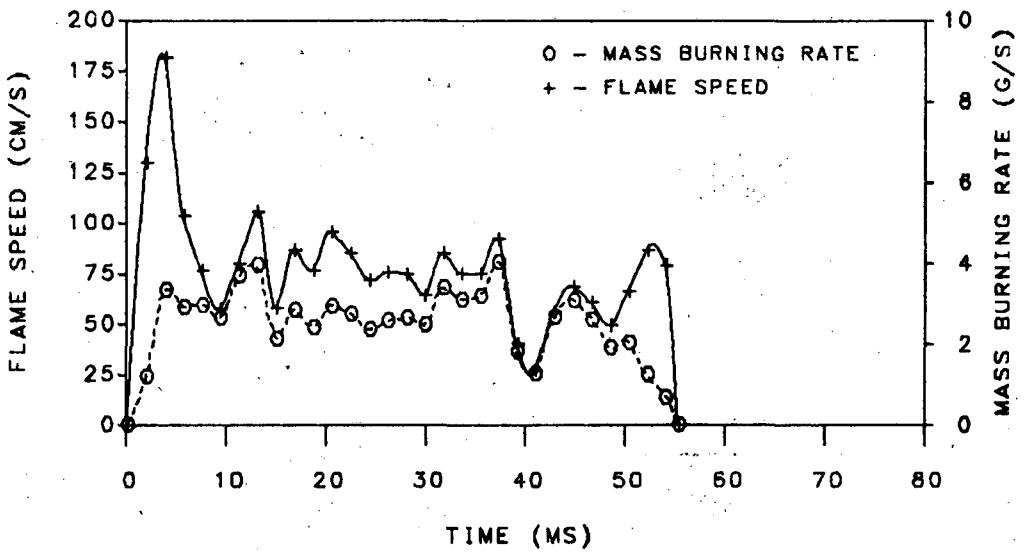

c) Flame speed and mass burning rate.

Figure 10. Methane/air flame results. Duct length = 90 mm; equivalence ratio = 1.0; time step between flame shape contours = 1.85 ms.

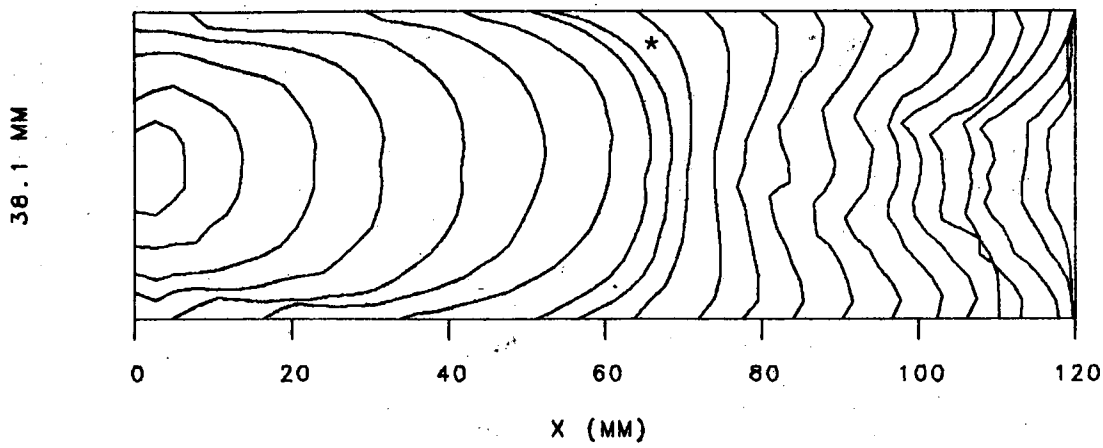

a) Flame shape.

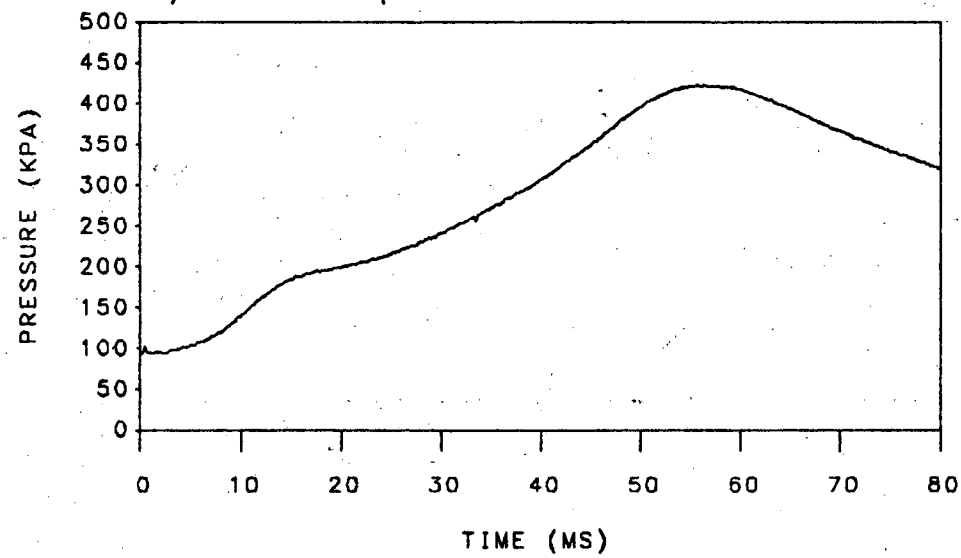

b) Pressure.

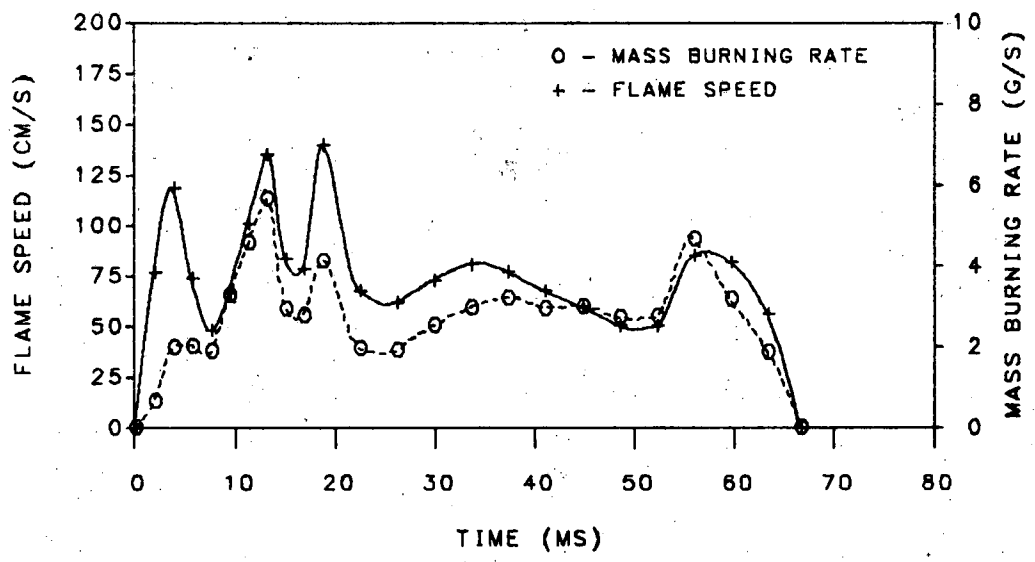

c) Flame speed and mass burning rate.

Figure 11. Methane/air flame results. Duct length = 120 mm; equivalence ratio = 1.0; time step between flame shape contours = 1.86 to * then 3.72 ms.

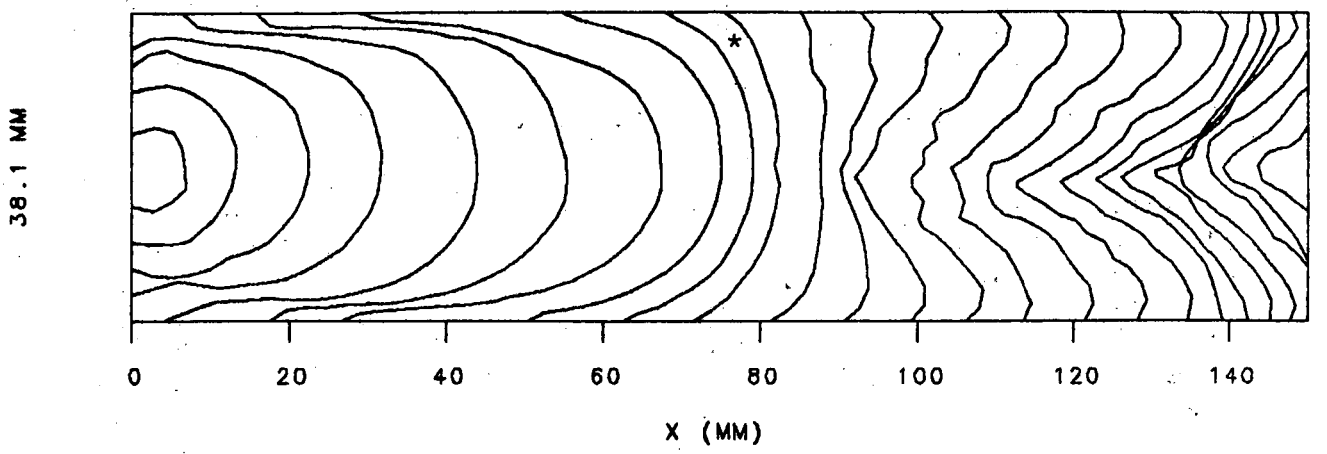

a) Flame shape.

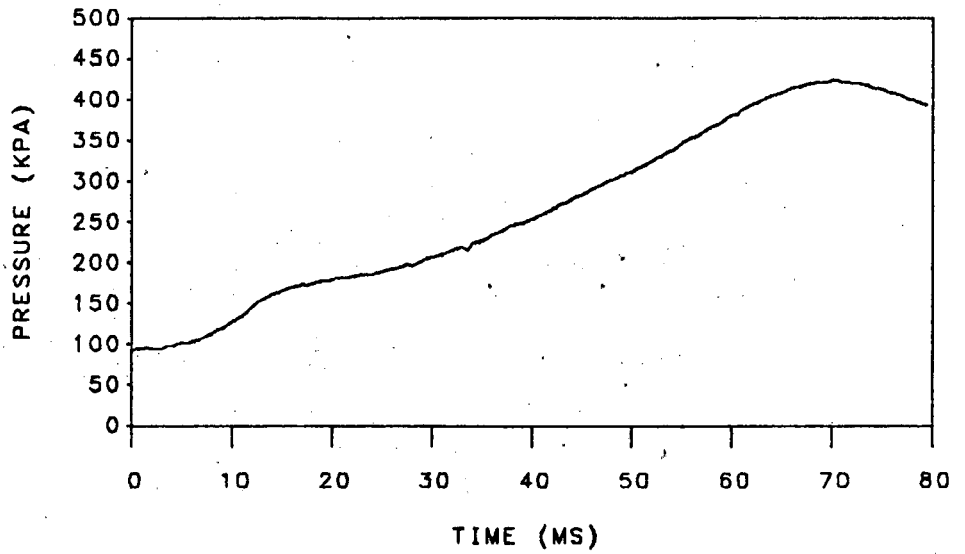

b) Pressure.

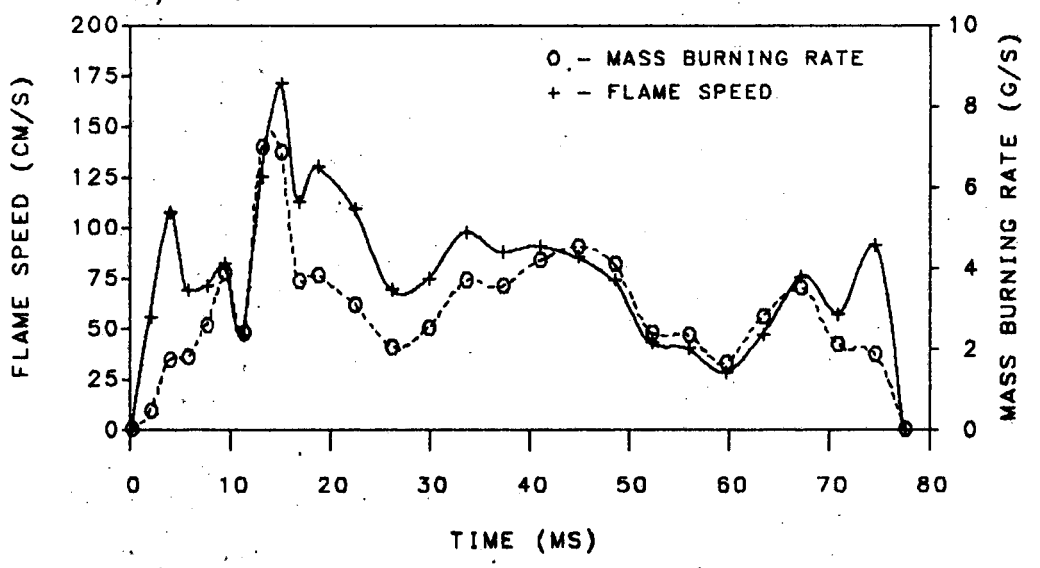

c) Flame speed and mass burning rate.

Figure 12. Methane/air flame results. Duct length = 150 mm; equivalence ratio = 1.0; time step between flame shape contours = 1.85 ms to * then 3.70 ms.

transition occurs at or just beyond the planar stage and is related to an increase in the apparent flame area.

c) The final peak occurs when the flame encounters the endwall. The endwall extinguishment rapidly reduces the flame area. The extreme peaks in the 30 mm and 60 mm cases are caused by large uncertainties in flame area. These uncertainties result from obscurity of the schlieren record at the end of small volume combustion. The mass burning rate is a better indicator of flame behavior in these final gases to burn.

The peak pressure is found to be nearly equal for all duct lengths, Figure 13. This is as expected as the peak pressure should be nearly proportional to energy per unit volume, and the energy per unit volume was held constant in all tests.

The time to peak pressure, Figure 13, is found to be a linear function of duct length over the range tested, 30 mm to 150 mm. This result seems to indicate that despite distinct differences in flame shape development the mean mass consumption rate is not sensitive to duct length.

Duct length has an effect on maximum flame speed, Figure 13. Both short and long ducts exhibit relatively high flame speed maxima while the middle lengths give lower results. The lowest maximum occurs for a 90 mm duct. The possible reasons for this local minimum have not been investigated.

There is a wealth of information in the literature on methane flame speeds as functions of equivalence ratio, temperature, and pressure. The reported maximum methane laminar flame speed for room temperature and atmospheric pressure is approximately 40 cm/s (Rallis and Garforth, 1980; Andrews and Bradley, 1972a; Andrews and Bradley, 1972b). In the present work a time history of flame speed has been determined for flames interacting with walls while the remaining pre-mixture undergoes adiabatic compression. The rather large possible error in flame area, due in part to the averaging scheme used and in part to deviation of the flame front from horizontal isotropy, make the reported flame speed magnitudes somewhat uncertain. This fact, with the unknown influences of wall heat transfer and mixture heating from compression, coupled with an often disturbed flame front, make comparison to the laminar flame speed difficult. Flame disturbance generally leads to flame speeds higher than for the purely laminar flames while wall interaction leads to lower flame speeds (Andrews and Bradley, 1972a; Linnett, 1953). One comparable case, work done by Woodard, at al. (1981) on the present apparatus, is in fair agreement, Figure 13.

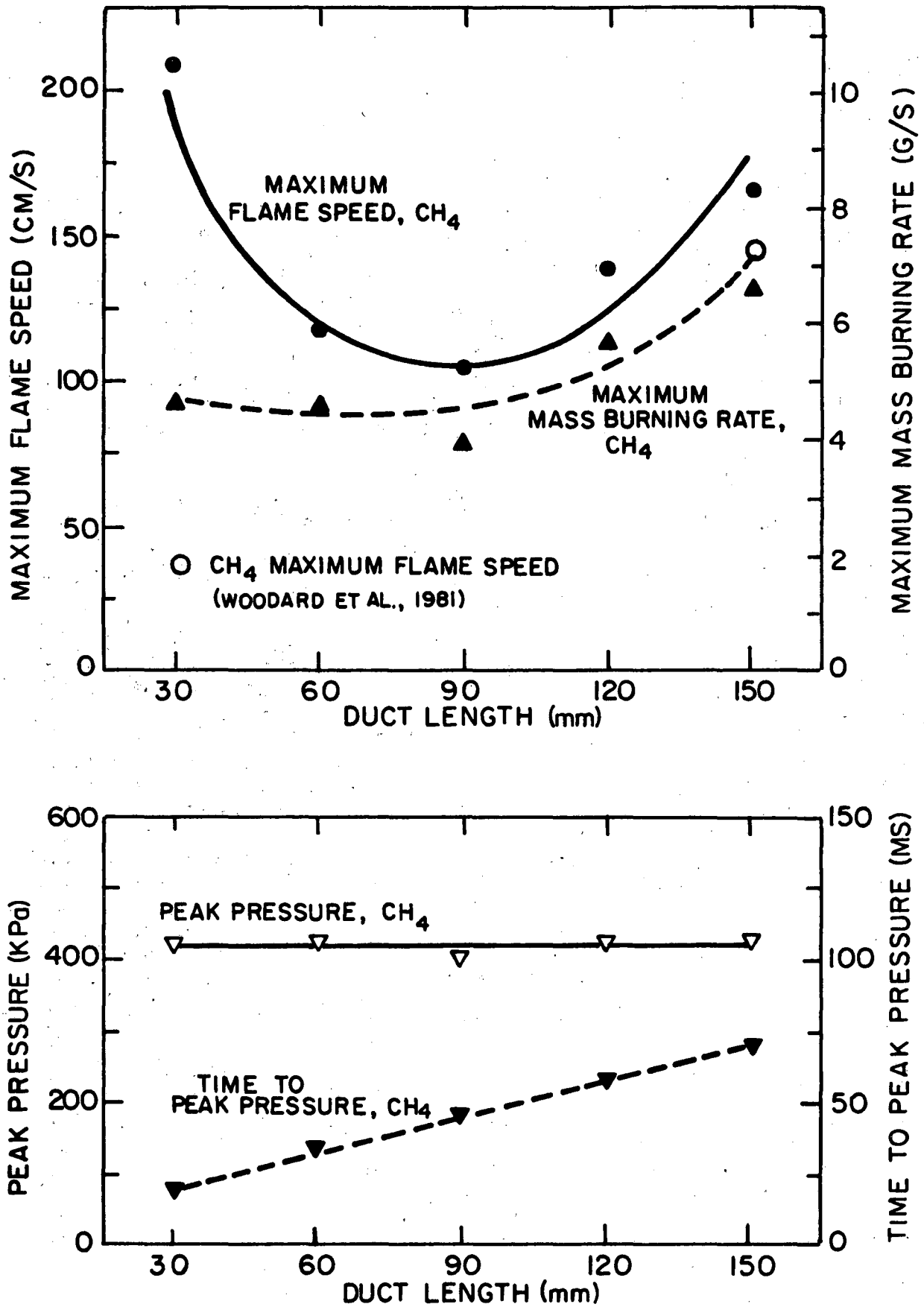

Figure 13. Peak results of methane/air flames versus duct length. Equivalence ratio 1.0. Peak flame speeds exclude results at the beginning and end of combustion.

ETHYLENE/AIR FLAME PROPAGATION: EFFECT OF EQUIVALENCE RATIO

Ethylene/air flames of various equivalence ratios (0.6-1.1) are studied, in continuation of the work completed by Woodard, et al. (1981) on methane/air flames. Ethylene was chosen for its higher laminar burning veloicty, about 80 cm/s (Gibbs and Calcote, 1959; Linnett and Hoare, 1949; Zabetakis, 1965), as compared with about 40 cm/sec for methane (Rallis and Garforth, 1980; Andrews and Bradley, 1972a, 1972b). A comparison of two fuels with significantly different flame speeds in terms of schlieren flame shapes, simultaneous pressure data and time resolved flame speeds and mass burning rates is sought. The experimental results for ethylene/air combustion are shown in Figures 14-19.

The ethylene flames behave qualitatively the same as the methane flames reported both in this work and in the previous study by Woodard, et al. (1981). The ethylene flames demonstrate the characteristic semi-cylindrical, planar, and folded shapes of the methane flames.

Both the semi-cylindrical and planar shapes were found to be virtually indistinguishable in shape from their methane counterparts. The folded region of the ethylene flames is not as prounounced as in the 150 mm methane case, Figure 12. The folded ethylene flames, however, display considerably more turbulent character than the methane flames. Wrinkled flame fronts are more evident for near stoichiometric flames. The turbulent character of the flames is found to be even more evident in the schlieren movies than in the average digitized flame shapes. For low equivalence ratios, 0.6 and 0.7, the folded flame departs from bilateral symmetry, Figures 18 and 19. Vertical flame propagation experiments, such as those of Coward and Hartwell (1932), indicate that the deviation is a buoyancy effect. Recent numerical calculations of horizontal flame propagation without gravitational forces (Cloutman, 1982) support the buoyancy supposition.

Ethylene pressure data show the same five regions as the methane pressure data and the pressure regions correspond to the same flame development as discussed in the methane case. In the ethylene experiments the steepness of the rising regions 1b) and 3) decreases with reduced equivalence ratio. The peak pressure also decreases as the equivalence ratio is lowered, Figure 20. The time to peak pressure shows the reverse behavior, decreasing for increasing equivalence ratio.

This behavior occurs because the energy per unit volume at lower equivalence ratios is smaller. Additionally, as equivalence ratio is reduced, heat losses become larger as the duration of the event increases.

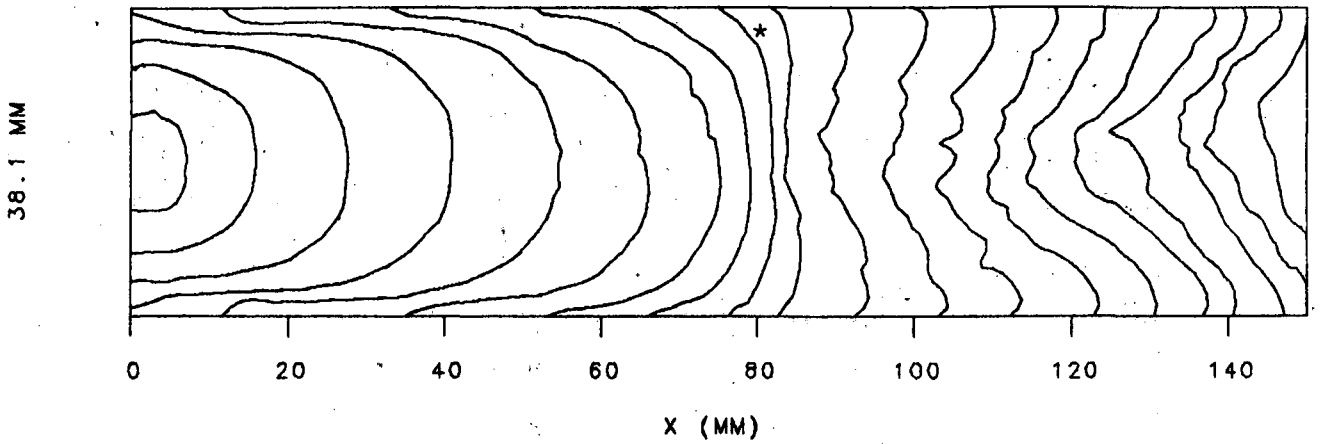

a) Flame shape.

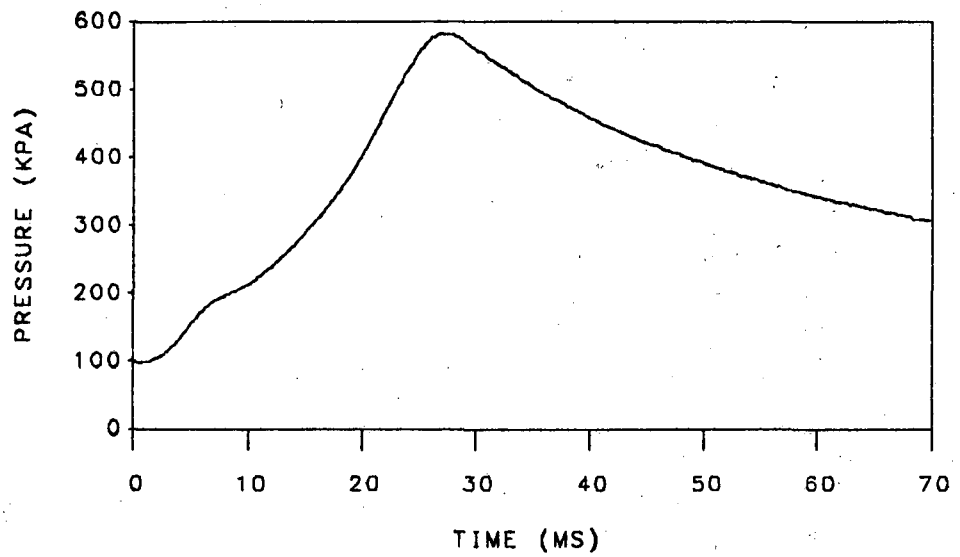

b) Pressure.

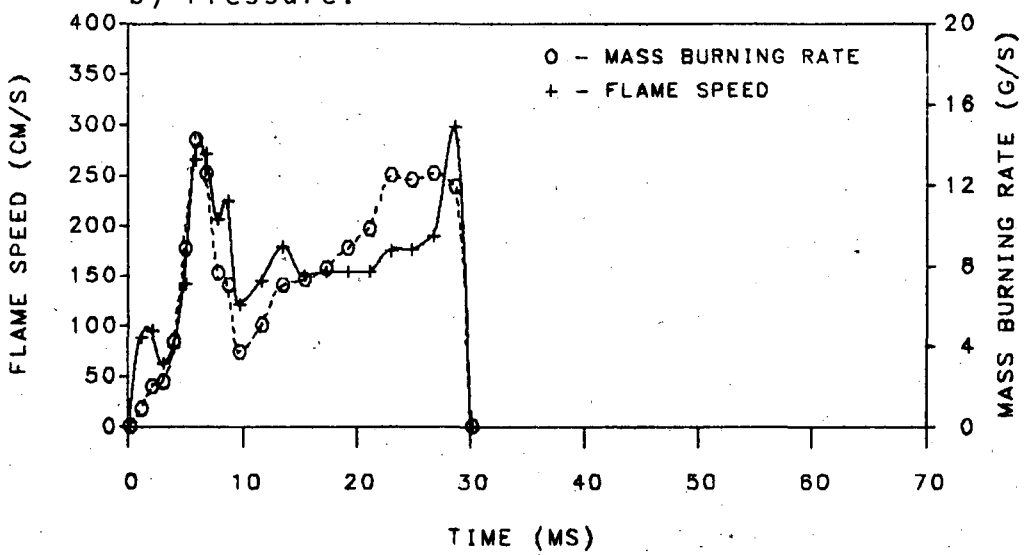

c) Flame speed and mass burning rate.

Figure 14. Ethylene/air flame results. Duct length = 150 mm; equivalence ratio = 1.0 time step between flame shape contours = 0.93 ms to * then 1.86 ms.

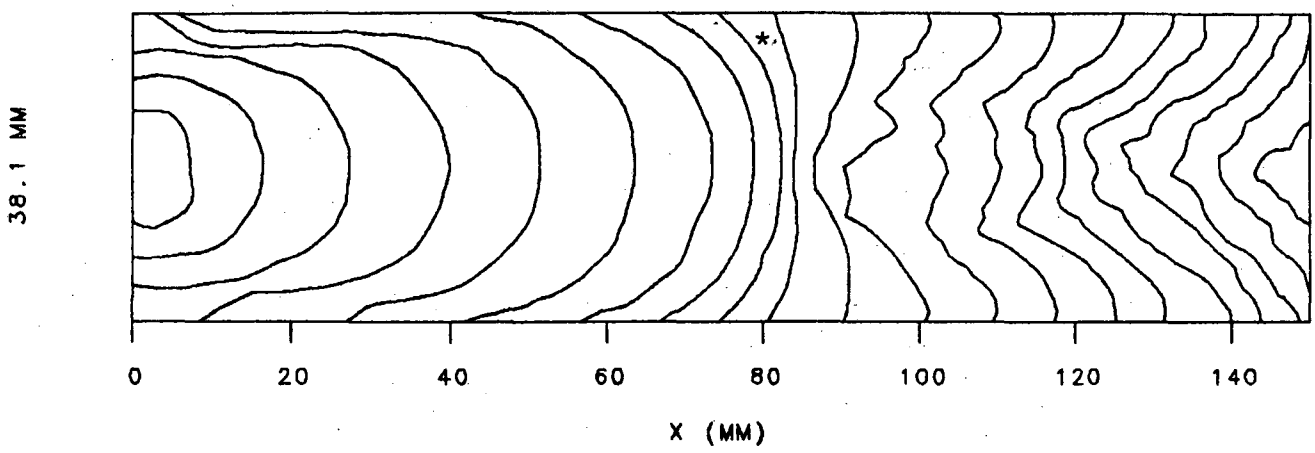

a) Flame shape.

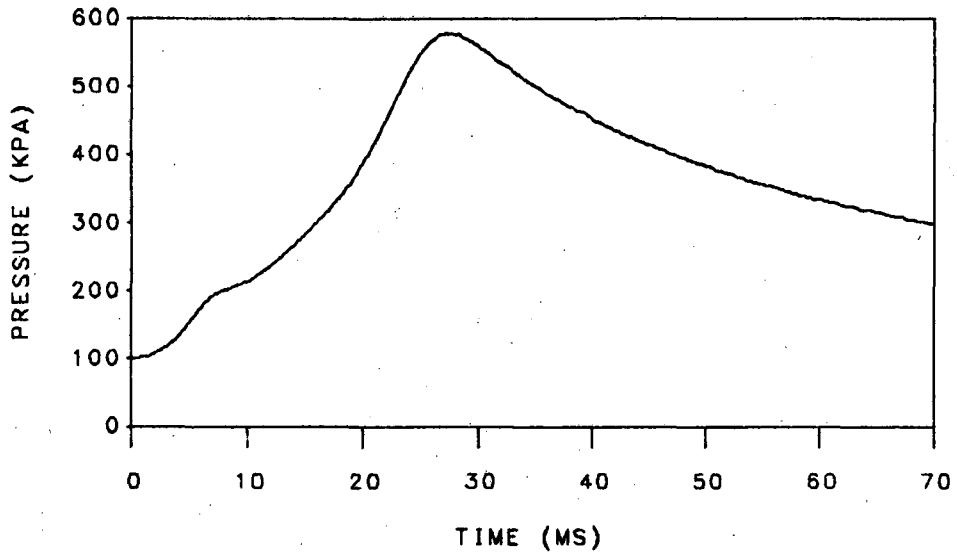

b) Pressure

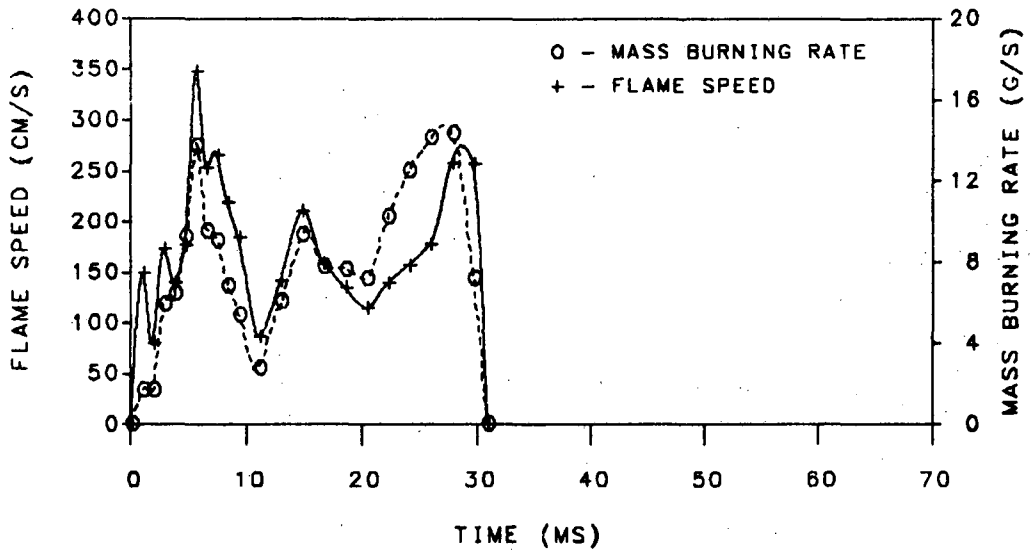

c) Flame speed and mass burning rate.

Figure 15. Ethylene/air flame results. Duct length = 150 mm; equivalence ratio = 1.0; time step between flame shape contours = 0.92 ms to * then 1.84 ms.

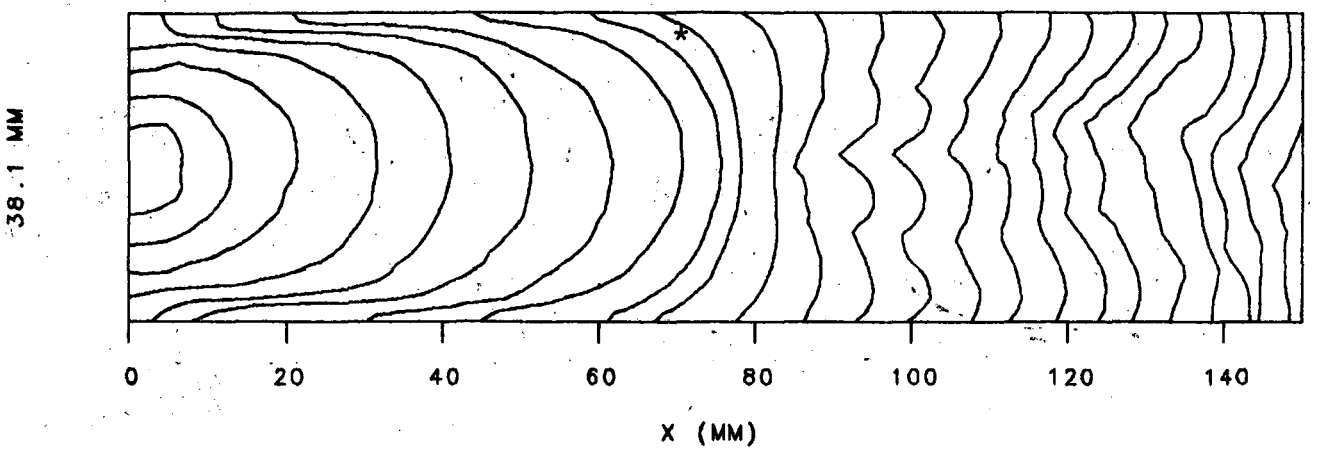

a) Flame shape.

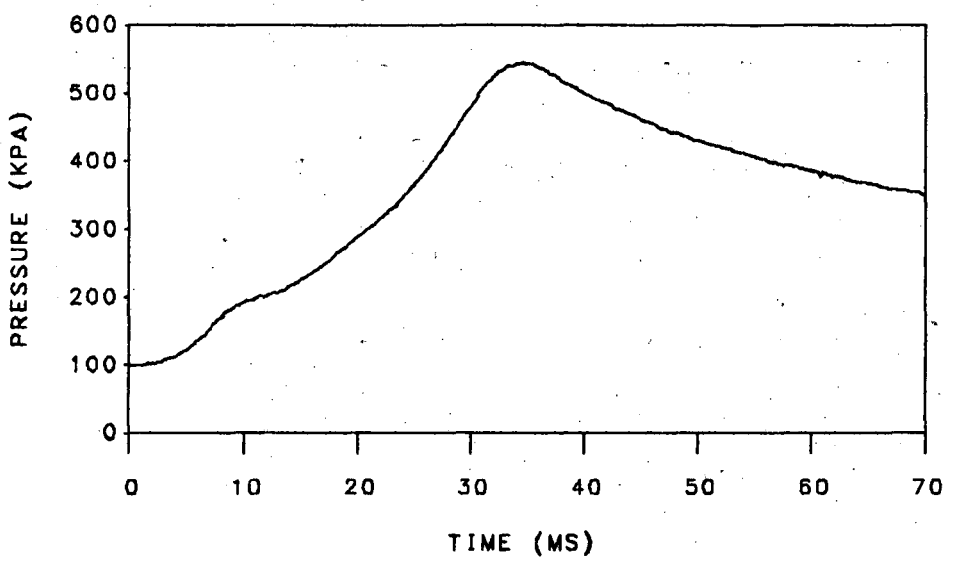

b) Pressure.

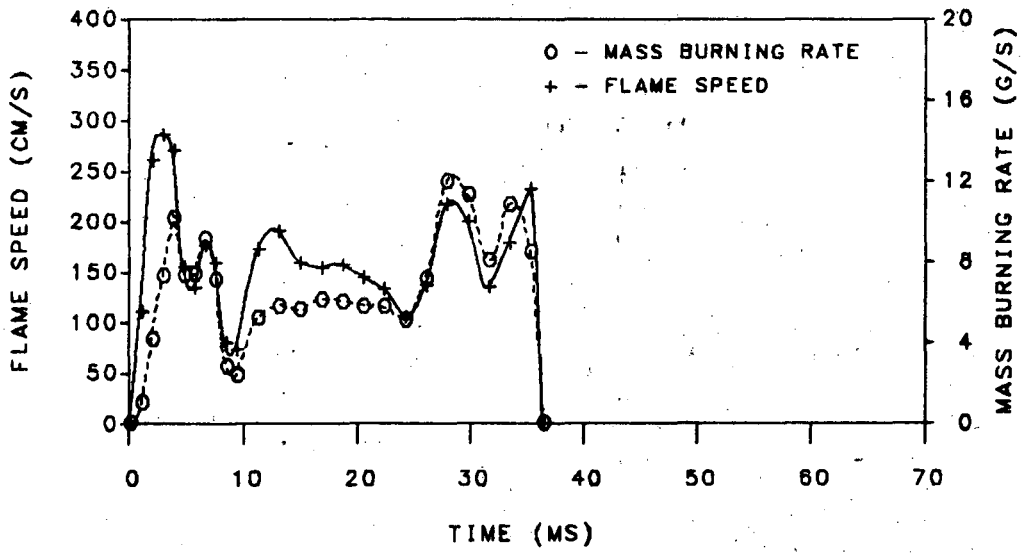

c) Flame speed and mass burning rate.

Figure 16. Ethylene/air flame results. Duct length = 150 mm; equivalence ratio = 0.9 time step between flame shape contours = 0.93 ms to * then 1.86 ms.

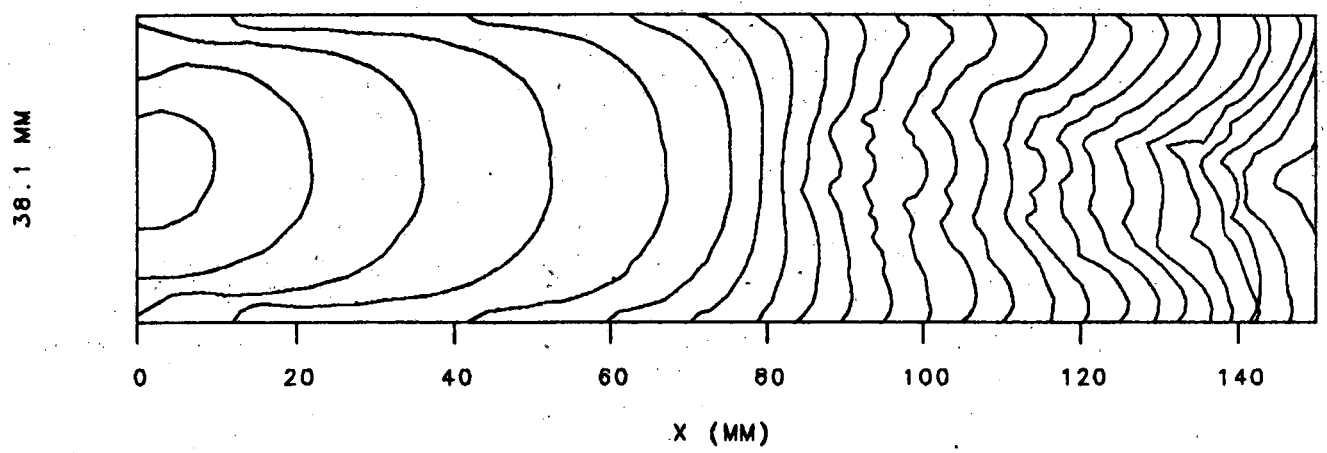

a) Flame shape.

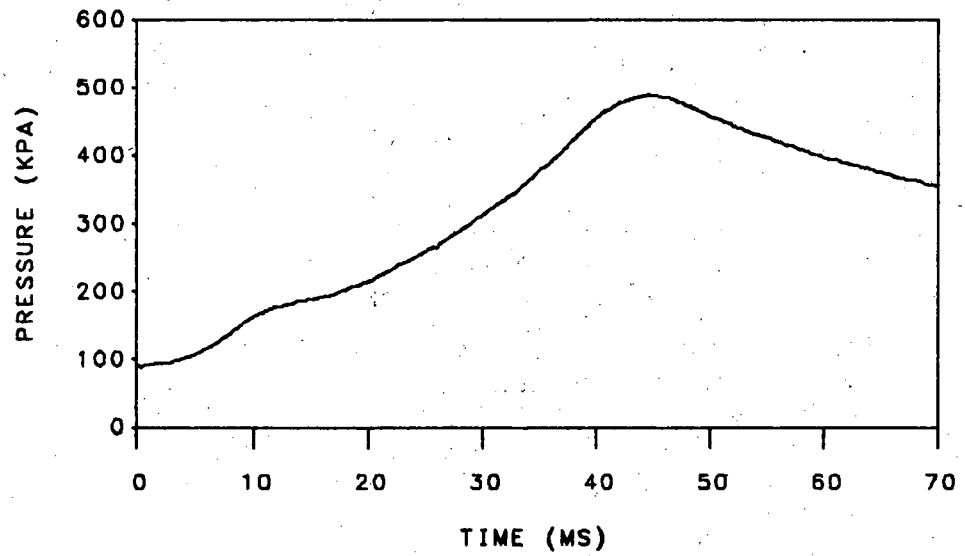

b) Pressure.

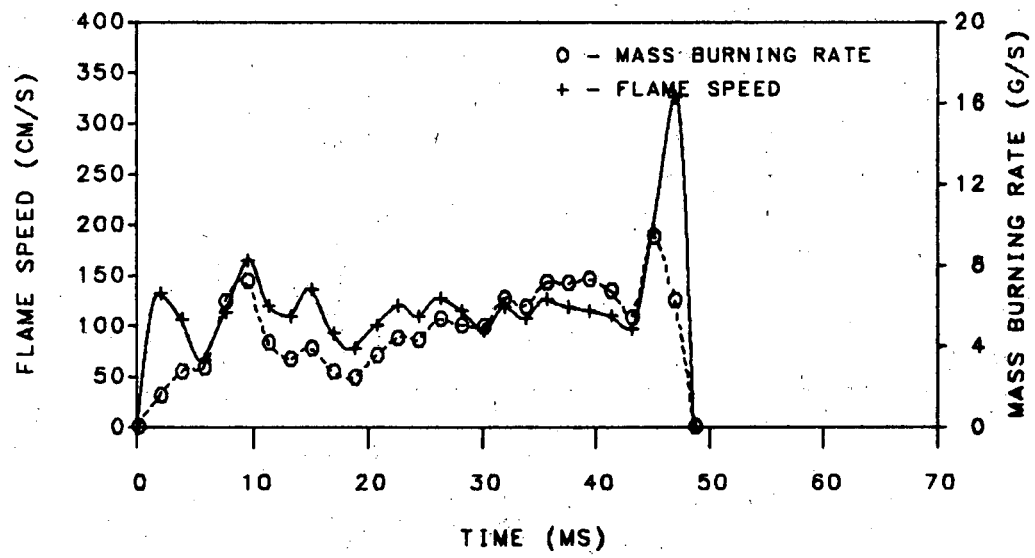

c) Flame speed and mass burning rate.

Figure 17. Ethylene/air flame results. Duct length = 150 mm; equivalence ratio = 0.8 time step between flame shape contours = 1.87 ms.

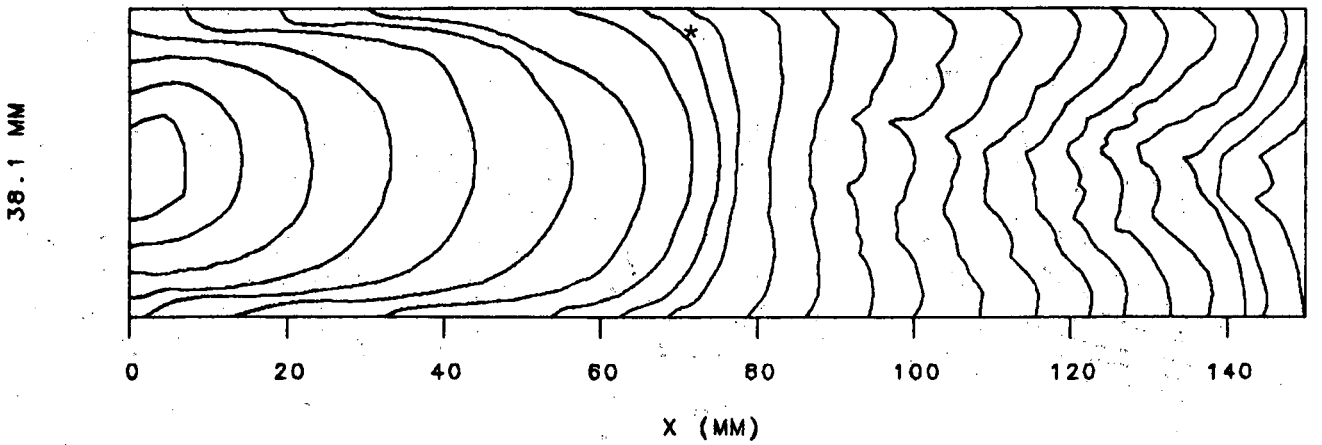

a) Flame shape.

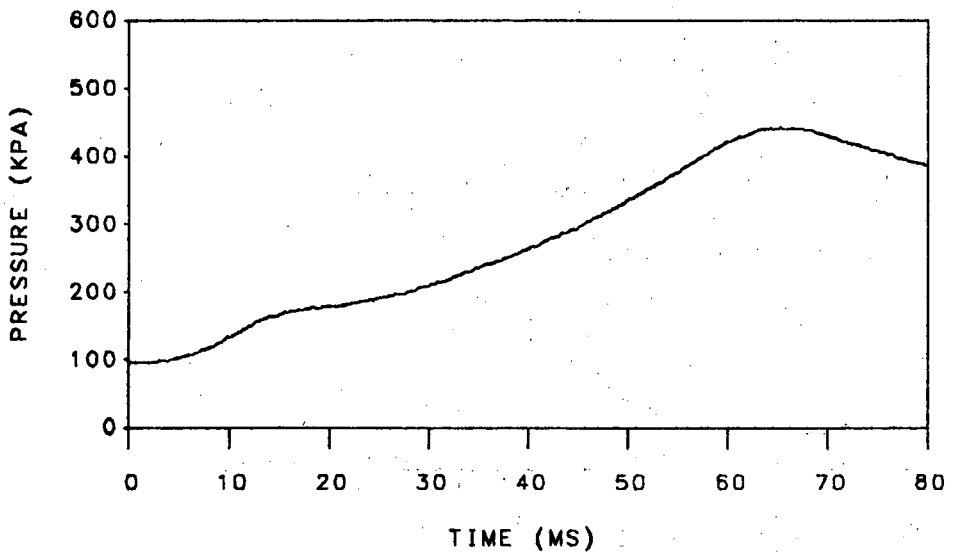

b) Pressure.

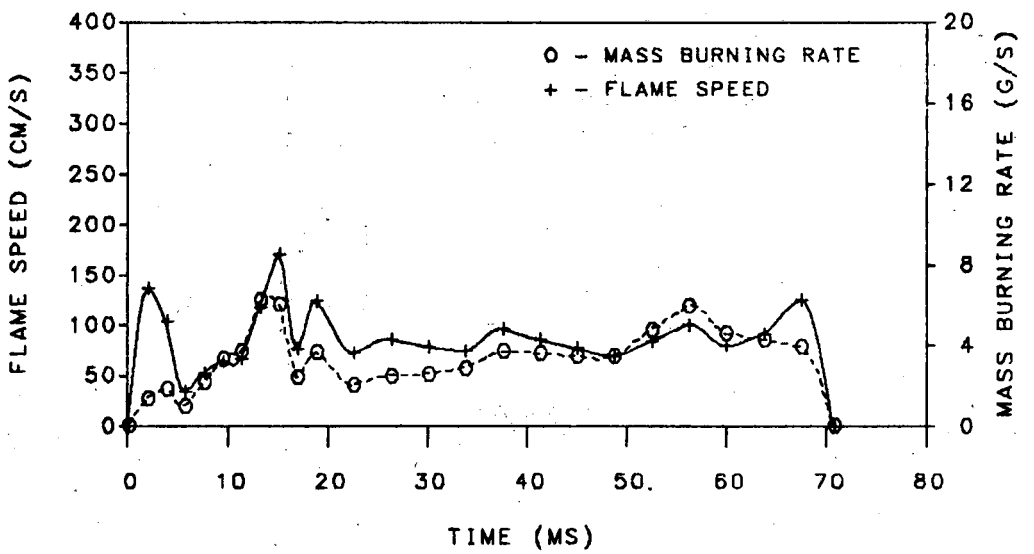

c) Flame shape and mass burning rate.

Figure 18. Ethylene/air flame results. Duct length = 150 mm; equivalence ratio = 0.7 time step between flame shape contours = 1.87 ms to * then 3.74 ms.

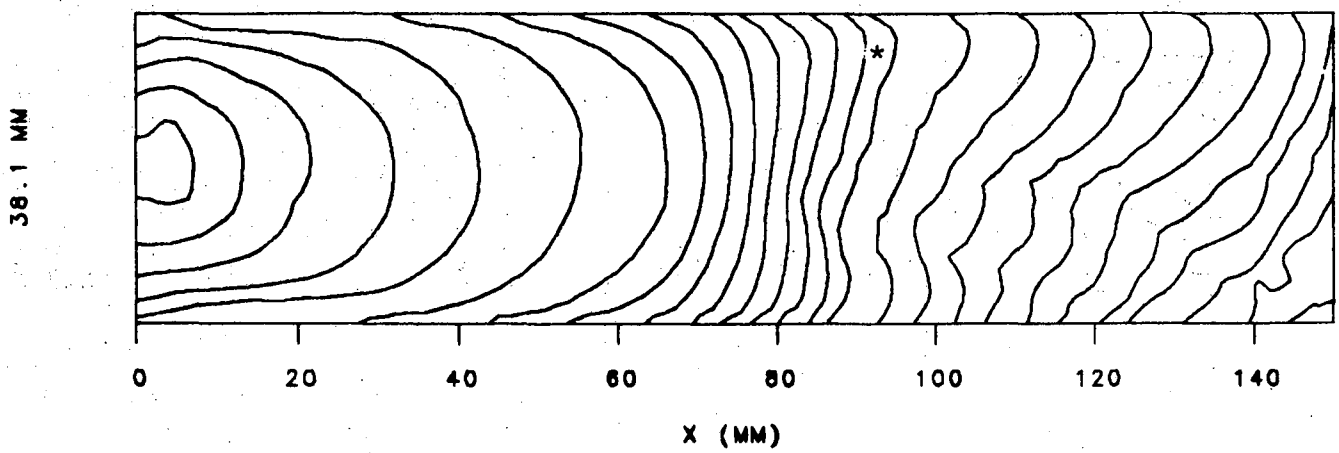

a) Flame shape.

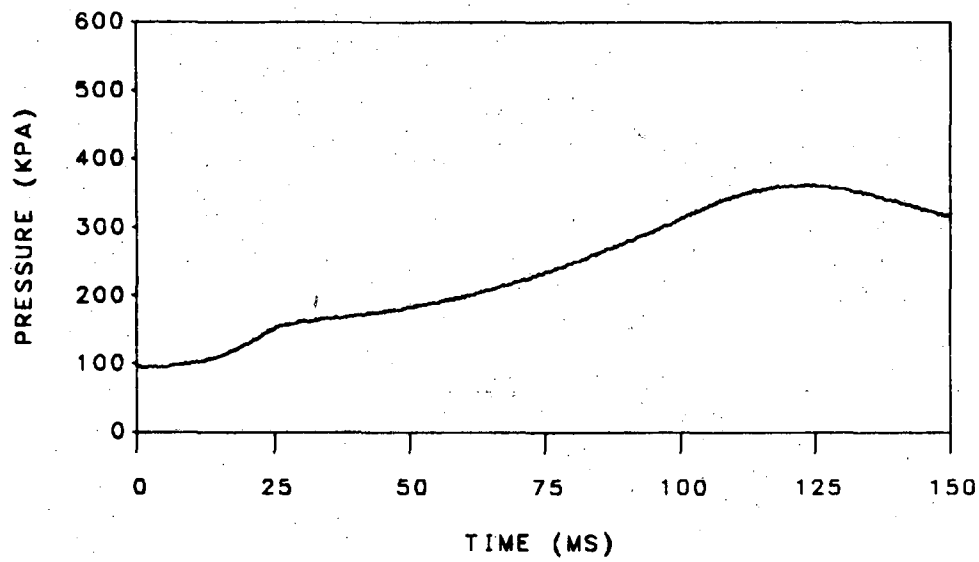

b) Pressure.

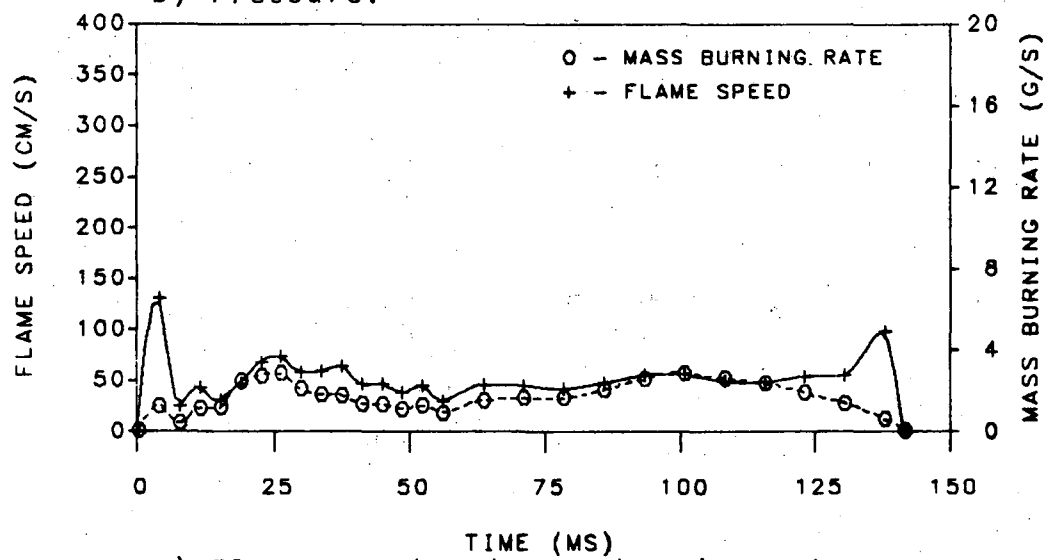

c) Flame speed and mass burning rate.

Figure 19. Ethylene/air flame results. Duct length = 150 mm; equivalence ratio = 0.6 time step between flame shape contours = 3.72 ms to * then 7.43 ms.

As expected, the combustion proceeds faster as the equivalence ratio increases to 1.1, in agreement with the reported peak in ethylene flame speed on the rich side of schoichiometric equivalence ratios (Gibbs and Calcote, 1959). The large increase in time to peak pressure for an equivalence ratio of 0.6 is believed due to the approach to the apparatus ignition limit. The reported ethylene/air ignition limit is 0.41 (Zabetakis, 1965) but heat transfer effects in the present apparatus prevent ignition at equivalence ratios lower than about 0.55.

The flame speeds and mass burning rates calculated for ethylene are found to be qualitatively the same as in the methane case. The four to five peaks reported for methane were found to be more distinct in the ethylene results, Figures 14-19. The persistence of the peaks through all tests indicates that they are perhaps due more to the geometry of the duct than to fuel composition. As with methane, ethylene displays significant flame speed peaks early and a single usually lower peak just before the flame extinguishes. The peak pressure is again observed to occur before the average flame extinguishes.

The functional dependence of the maximum flame speed and mass burning rate (excluding peaks at the beginning and end of combustion due to uncertainties) on equivalence ratio shows the same tendency as the pressure maxima, Figure 20. The maxima increase as mixtures become richer. This tendency agrees with the reported behavior of laminar ethylene flame speeds, Gibbs and Calcote (1959). The absolute values of the literature results and the present results are not expected to be comparable due to the significant differences in experimental conditions as previously explained.

A comparison of ethylene results is made to results obtained for methane on the same apparatus by Woodard, et al. (1981). The ethylene flame speeds show the same trends as methane but are greater by about a factor of two, Figure 20. This ratio matches fairly closely that reported in the literature for laminar flame speeds.

CONCLUSIONS

A study is made of flames propagating in a constant volume duct. Simultaneous high-speed schlieren movies and pressure data are obtained for methane/air and ethylene/air flames. The effects of duct length on methane/air flames and the effects of equivalence ratio on ethylene/air flames are reported. An average of front and rear schlieren images is found to be the most tractable definition of the flame front location.

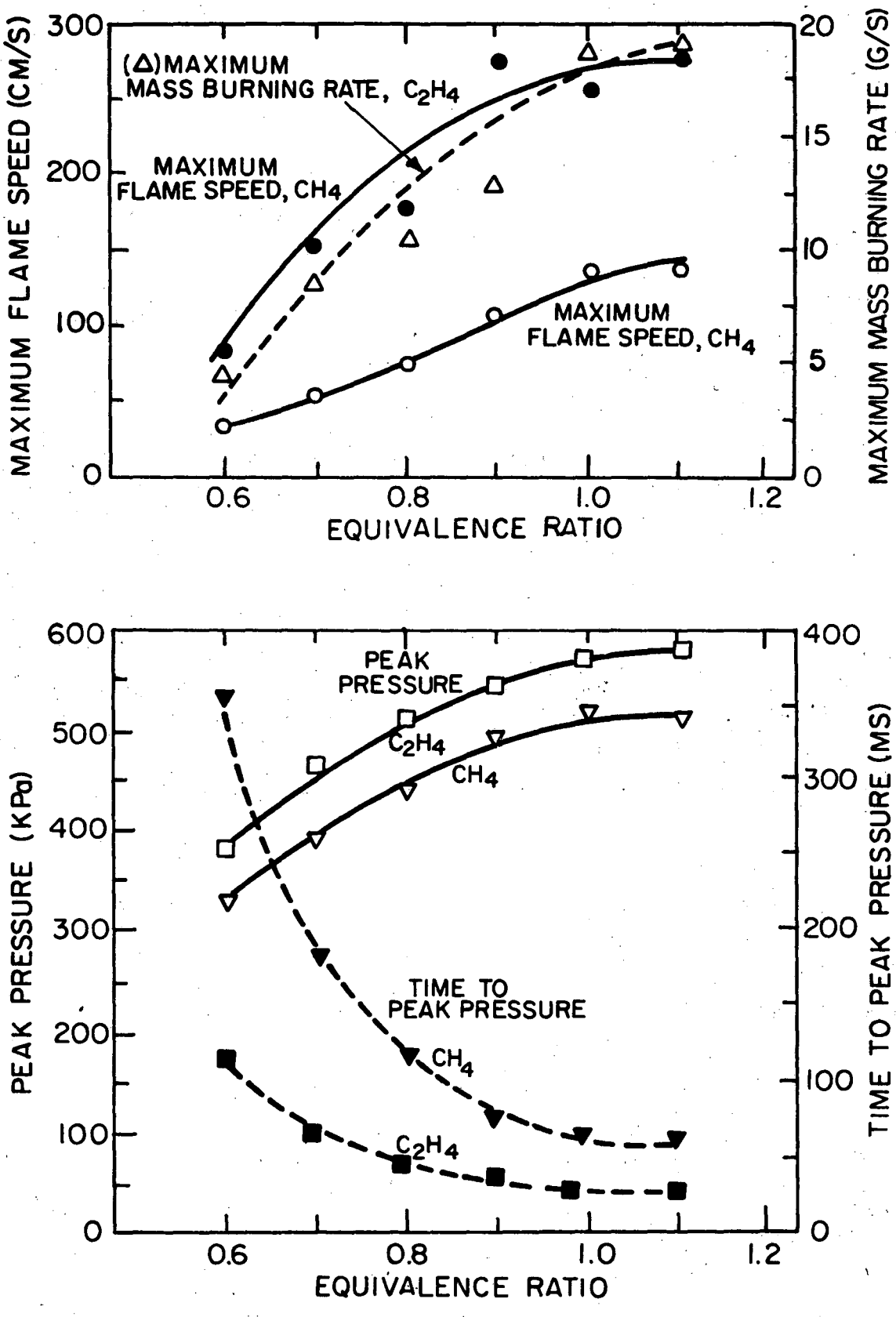

Figure 20. Peak results of ethylene/air and methane/air flames. Duct length = 150 mm. Peak flame speeds exclude the results at the beginning and end of combustion.

Specific consideration is given to the inter-relationship between flame shape, combustion chamber pressure, and flame speed. The salient features of this comparison are:

1) All flames studied demonstrate a definite flame shape development.
2) Despite different combustion properties, the flame shape development for stoichiometric flames of both methane and ethylene are found to be nearly identical.
3) Ethylene/air flame shape sensitivity to equivalence ratio is primarily a buoyancy effect. Low flame speeds near the lean flammability limit allow bouyant forces to alter significantly the flame shape.
4) The methane/air flame shape development is found to depend strongly on the length of the duct. Flames in shorter ducts (30 mm and 60 mm) do not demonstrate folding.
5) The mean mass consumption rate in methane/air flames is independent of differences in flame shape development.
6) A strong correlation exists between flame shape and pressure behavior. A similar correlation is not found between flame shape and flame speed.

Flame speeds alone are also investigated. The salient points of the flame speed analysis are:

7) Flame speeds at the beginning and end of the combustion event have large uncertainties.
8) Peak flame speed of ethylene/air flames demonstrates an expected increase with increasing equivalence ratio, up to 1.1. Surprisingly, stoichiometric methane/air flames show a peak flame speed minimum at the middle duct length tested.
9) Peak flame speeds for ethylene/air mixtures are found to be approximately a factor of two greater than for methane/air mixtures.

Future work will pursue a closer simulation of internal combustion engines by introducing piston motion into the experiments. Piston induced fluid motion is expected to dominate the flame behavior and to provide an informative comparison with flame propagation at constant volume.

ACKNOWLEDGEMENTS

The authors appreciate the extensive assistance provided by Ken Hom in the preparation of the apparatus and conduction of the experiments. Gary Hubbard developed much of the data logging software. This work was supported by the Lawrence Laboratory under U.S. Department of Energy Contract DE-AC03-76SF0098. Support for W. Steinert was provided by the Deutsche Forschungsgemeinschaft.

REFERENCES

Andrews, G.E. and Bradley, D. (1972a). Determination of burning velocities: a critical review. Combustion and Flame, 18, 133-153.

Andrews, G.E. and Bradley, D. (1972b). The burning velocity of methane-air mixtures. Combustion and Flame, 19, 275-288.

Coward, H.F. and Hartwell, F.J. (1932). Studies in the mechanism of flame movement. Part I. The uniform movement of flame in mixtures of methane and air, in relation to tube diameter. Journal of the Chemical Society, 1996-2004.

Cloutman, L.D. (1982). Personal Communication. Los Alamos National Laboratory, Theoretical Division.

Dale, J.D., and Oppenheim, A.K. (1982). A rationale for advances in the technology of I.C. Engines. SAE Paper No. 820047.

de Soete, G.G. (1981). Measurement of initial flame speed by laser tomography. First Specialists Meeting (International) of the Combustion Institute, Bordeaux, France, July 20-24.

Gibbs, G.J. and Calcote, H.F. (1963). Effect of molecular structure on burning velocity. Journal of Chemical Engineering Data, 4, 226-237.

Guenoche, H. (1964). Flame propagation in tubes and in closed vessels. In Non-steady Flame Propagation, G. Markstein (Editor), Pergamon Press, New York.

IME (1979). Fuel Economy and Emissions of Lean Burn Engines. Institution of Mechanical Engineers Conference, Publication 1979-9, London, June 12-14.

Lewis, B. and von Elbe, G. (1961). Combustion, Flames and Explosions of Gases, Chapter 5, Sections 9-11. Academic Press, New York.

Linnett, J.W. (1953). Methods of measuring burning velocities. Fourth Symposium (International) on Combustion, 20-35. Williams and Wilkens, Baltimore.

Linnett, J.W. and Hoare, M.F. (1949). Burning velocities in ethylene-air-nitrogen mixtures. Third Symposium on Combustion, Flames and Explosion Phenomena, 195-204.

Markstein, G. (Editor) (1964). Non-steady flame propagation. Pergamon Press, New York.

Noguchi, M., Landa, L., and Nakamura, N. (1976). Development of Toyota Lean Burn Engine. SAE Paper No. 760757, SAE Transactions 1976, Section 4.

Oppenheim, A.K., Cheng, R.K., Teichman, K. Smith, I.O., Sawyer, R.F., Hom, K., and Stewart, H.E. (1976). A cinematographic study of combustion in an enclosure fitted with a reciprocating piston. In Stratified Charge Engines, Institution of Mechanical Engineers Conference Publications 1976-11, 127-135.

Rallis, C.J. and Garforth, A.M. (1980). The determination of laminar burning velocity. Progress in Energy and Combustion Science, 6, 303-329.

Shiomoto, G.H., Sawyer, R.F. and Kelly, B.D. (1978). Characterization of the lean misfire limit. SAE Paper No. 780235.

Smith, O.I. (1977). Lean limit combustion in an expanding chamber. Lawrence Berkeley Laboratory Report No. LBL-6851, PhD Thesis.

Smith, O.I., Westbrook, C.K., and Sawyer, R.F. (1979). Lean limit combustion in an expanding chamber. Seventeenth Symposium (International) on Combustion, 1305-1313. The Combustion Institute, Pittsburgh.

Weinberg, F.J. (1963). Optics of Flames. Butterworths, London.

Woodard, J.B., Hirvo, D.H., Greif, R., and Sawyer, R.F. (1981). Wall heat transfer and flame propagation in a constant volume duct. Western States Section/The Combustion Institute Paper No. 81-51 and Lawrence Berkeley Laboratory Report No. LBL-13021.

Zabetakis, M.G. (1965). Flammability characteristics of combustible gases and vapors. Bureau of Mines, Bulletin 627.

TECHNICAL INFORMATION DEPARTMENT
LAWRENCE BERKELEY LABORATORY
UNIVERSITY OF CALIFORNIA
BERKELEY, CALIFORNIA 94720